Thesis for the degree of doctor of philosophy

Mechanisms of adhesive mixing for drug particle inhalation

Numerical investigation of the interplay between formulation variables

MOHAMMADREZA TAMADONDAR

CHALMERS
UNIVERSITY OF TECHNOLOGY

Department of Chemistry and Chemical Engineering
Chalmers University of Technology
Göteborg, Sweden 2020

Mechanisms of adhesive mixing for drug particle inhalation
Numerical investigation of the interplay between formulation variables

Mohammadreza Tamadondar

ISBN 978-91-7905-314-7

Supervisor: Anders Rasmuson

Doktorsavhandlingar vid Chalmers tekniska högskola,
Ny seri nr 4781
ISSN 0346-718X

Department of Chemistry and Chemical Engineering
Chalmers University of Technology
SE-412 96 Göteborg, Sweden
Telephone: +46 (0)31 772 1000

Cover: The image shows how the adhesive mixing fits into the overall process of lung drug delivery via inhalation. The image of the adhesive mixture is the direct outcome of the numerical study that is carried out in the present research. The critical attributes of the mixing process, including shape, roughness, and presence of fine excipient particles are outlined, which have been thoroughly studied in this work.

Printed by Chalmers Reproservice
Göteborg, Sweden (2020)

Mechanisms of adhesive mixing for drug particle inhalation
Numerical investigation of the interplay between formulation variables

Mohammadreza Tamadondar
Department of Chemistry and Chemical Engineering
Chalmers University of Technology

Abstract

Formulation of therapeutic dry powders for lung drug delivery via inhalation is done via **adhesive mixing**. In this process, micron-sized active pharmaceutical ingredient particles are blended with relatively coarse carrier particles until stable **adhesive units** of carrier and drug particles are formed. Inside an inhaler and upon its actuation, the turbulent kinetic energy of the air stream is transferred to the bulk powder of adhesive units and, consequently, drug particles are dispersed into primary respirable particles. The formulation process – in addition to the inhaler design and the patient's respiratory maneuver - is one of the three pillars that determine the overall performance of this form of drug administration, and therefore, it must be genuinely understood. Despite all the recent advancements in the formulation of carrier-based dry powder inhalers, the *in vitro* efficiency of currently marketed inhalers is at best less than 50% of their nominal values [2017].
The goal of this research is to devise a methodology to comprehend the complex nature of the adhesive mixing process for inhalation and to optimize this process. The small temporal and spatial scales of the adhesive mixing, on the one hand, and the omnipresent interplay of process variables, on the other hand, require a modeling framework and several quality-assessment tools. The underlying principle of this framework is to treat the adhesive mixture as a particulate system, whose dynamic behavior can be modelled by applying Newton's laws of motion to individual particles.
Several formulation variables are selected, in accordance with their significance in the process and within the capacity of the developed model, for parameter studying. These variables include: (i) the adhesive properties of particles, (ii) mixing intensity, (iii) the shape of carriers, (iv) the surface asperity of particles, and (v) the added fine particles (ternary blend). The process quality is inferred from mixing homogeneity indices, the micro-scale structure of adhesive units, and the fragmentation analyses of drug agglomerates. In addition to the formulation process, simulated dispersion tests are performed in order to understand the role of carrier surface roughness on drug particle detachment during aerosolization. A combination of mixing energy and particle surface energies is used to map the mixing state. It is found that any imbalance between these two process variables results in poor adhesive mixtures. The non-sphericity of carrier particles is also shown to impose a noticeable difference in the breakage and adhesion pattern of drug agglomerates. In the context of formulation, carrier surface roughness reduces drug deposition, and in the context of dispersion, drug detachment is found to be proportional to the roughness length scale. Lastly, several cases of ternary formulations are simulated, and the relevance of the active site and the buffer theories are examined.

Keywords: Adhesive mixing, Agglomerate, Carrier Particle, Discrete Element Method, Dispersion, DPI-formulation.

In memory of
Rira Esmaeilion
Parisa Eghbalian
Pouneh Gorji
Arash Pourzarabi
Niloofar Ebrahim
Saeed Tahmasebi
Sara Mamani
Siavash Ghafouri-Azar
... and all the dear lives in PS752

List of Appended Papers

The thesis is based on the work reported in the following papers, referred to by Roman numerals in the text:

Paper I

Numerical modeling of adhesive particle mixing.
Tamadondar. M.R., Rasmuson. A., Thalberg. K., Niklasson Björn. I. AIChE Journal. 2017; 63(7):2599-2609

Paper II

The influence of particle interfacial energies and mixing energy on the mixture quality of the dry-coating process.
Tamadondar. M.R.,de Martín. L., Rasmuson. A., Thalberg. K., Niklasson Björn. I. Powder Technology. 2018;338:313-324

Paper III

Agglomerate breakage and adhesion upon impact with complex-shaped particles.
Tamadondar. M.R., de Martín. L., Rasmuson. A. AIChE Journal. 2019; 65(6):1-12

Paper IV

The effect of carrier surface roughness on wall collision-induced detachment of micronized pharmaceutical particles.
Tamadondar. M.R., Rasmuson. A. AIChE Journal. 2019; doi.org/10.1002/aic.16771

Paper V

The role of fine excipient particles in adhesive mixtures for inhalation.
Tamadondar. M.R., Rasmuson. A. Submitted to the AIChE Journal. 2020.

Author's contribution to the publications is as follows:

Paper I:
I designed and performed the DEM simulations. The results were analyzed together with co-authors. I am the main author of the paper.

Paper II:
The DEM simulations were conducted by the author, and the experimental data were provided by co-supervisors at AstraZeneca. The results were interpreted together with co-authors. I am the main author of the paper.

Paper III:
I designed the particle shapes and simulated the collision test in the DEM framework. Together with co-authors, I analyzed the results and wrote the manuscript.

Paper IV
I developed the numerical algorithm for surface roughness measurement and performed all the required simulations. The outcomes were examined together with the co-author. I am the main author of the paper.

Paper V
I performed the DEM simulations, and together with the co-authors, analyzed the results. I am the main author of the paper.

List of Acronyms

ANOVA	Analysis of Variance
API	Active Pharmaceutical Ingredient
BD	Brownian Dynamic
CAB	Cohesive-Adhesive Balance
DEM	Discrete Element Method
DMT	Derjaguin-Muller-Toporov
DPD	Dissipative Particle Dynamic
DPI	Dry Powder Inhaler
FPF	Fine Particle Fraction
JKR	Johnson-Kendall-Roberts
MD	Molecular Dynamic
MFV	Minimum Fluidization Velocity
ODEC	Overlapping Discrete Element Cluster
QM	Quantum Mechanics
rpm	revolutions per minute
SAC	Surface Area Coverage

Contents

List of Figures

List of Tables

1
Introduction

1.1 Adhesive mixing process

Mixing of interactive particles with a large size disparity is a common process to synthesize particles with tailored functionalities for a variety of industrial and technological applications. This process comprises blending adhesive fine and coarse particles in the absence of any binders, until the fine particles are distributed over the surfaces of coarse particles [2]. The ultimate mixture tends to have a higher degree of mixing homogeneity than random mixing of particles, because the intrinsic adhesion between two mixing components is normally large enough to overcome the weight of smaller particles and prevent segregation. Adhesive mixing bears resemblance to the concept of ordered mixing that was introduced by Hersey almost five decades ago [56]. This process can be described with the following essential steps [2]:

- The mixing starts when the agglomerates of fine particles attach to adjacent coarse particles and are carried around, i.e. the first coated carriers are created.
- When the agglomerates collide with or are compressed by coarse particles, they break apart, i.e. the agglomerates are fragmented.
- The continuous collision and friction of carriers deteriorate the remaining agglomerates and disperse fine particles onto the coarse surfaces, i.e. the coated area is increased.

A similar process has been adopted in the context of particles coating, primarily to find an alternative to the wet-coating of particles. Analogous to adhesive mixing, in the dry-coating process, large host particles are loosely covered with small guest particles with the objective of modifying particle flowability, solubility, hydrophobicity, and other surface properties. Contrary to the wet-coating methods, coating under dry conditions is environmentally benign, and more cost effective, and the method promises more versatile surface modifications [130].

1.2 Dry powder inhaler (DPI)

1.2.1 Formulation of DPI

One important utilization of the adhesive mixing process is the formulation of therapeutic powders for lung drug delivery via inhalation. The dynamic structure of human respiratory airways implies that only a narrow aerodynamic particle size range of roughly 1-5 μm can

lead to sufficient drug deposition in lung tracts [113]. Therefore, the efficacy of drug delivery via inhalation depends on fulfilling this constraint on particle size, despite the strong tendency of micron-sized particles toward enlargement due to agglomeration.
The practical solution to this challenge is incorporating relatively coarse **carrier** particles into the micron-sized active pharmaceutical ingredient (**API**) particles via blending. The formulation process results in the temporary adhesion of API particles with the surface of carriers, and this prevents drug agglomeration. The formation of **adhesive units** between carrier and API particles enhances powder flowability, and more importantly, promises an effective and reproducible drug dose upon aerosolization [24].

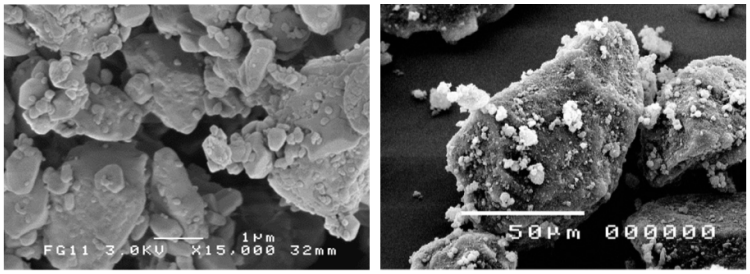

Figure 1.1: (Left) Aggregated micron-sized Budesonide API particles [52]; (Right) Formulation of Respitose SV003 as carrier and 5% Budesonide [114]

1.2.2 Dispersion mechanisms in DPI

The dispersion of adhesive mixtures upon inhalation transforms the bulk powder to aerosol form. Once the inhaler has been triggered, and airflow entrains through a DPI device (as a result of the patient's respiration), the static bulk powder is fluidized. The fluidization initiates the de-agglomeration process, wherein turbulent kinetic energy is transferred to the particles, and consequently, the API particles are stripped from carriers, and the small agglomerates of APIs are dispersed into primary respirable particles [34].
The de-agglomeration process is argued to be governed by two distinct mechanisms: (i) flow-induced and (ii) collision-induced dispersion. In flow-induced dispersion, the aerodynamic forces exerted by the airstream, including turbulent shear, drag, and lift forces, are responsible for particle detachment, while in collision-induced dispersion, the particle friction force and the inertial forces originating from interparticle and particle-wall collisions determine de-agglomeration [58].

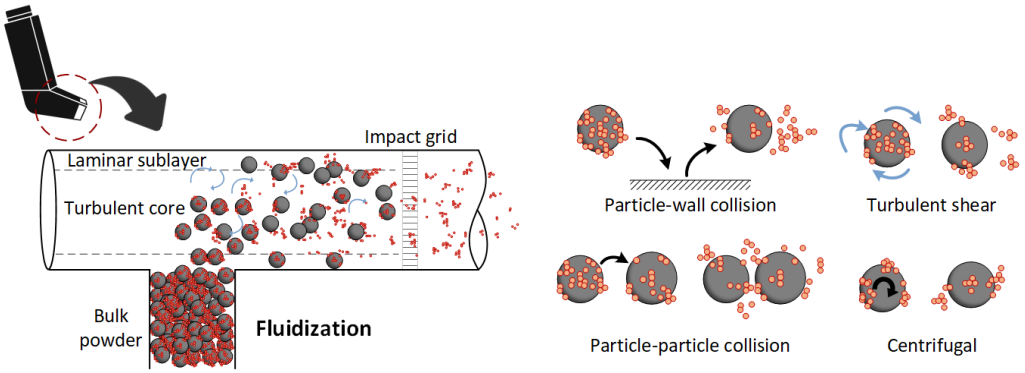

Figure 1.2: (Left) Schematic diagram of drug particle dispersion in an inhaler; (Right) Details of the dispersion mechanisms [58]

The efficiency of the dispersion process is commonly expressed as the weight fraction of API particles smaller than 5 m that are released from the inhaler. This fraction is therapeutically the most relevant indicator of DPI performance and is referred to as the fine particle fraction (FPF). The remaining fraction of drug particles may either remain as large aggregates or may stay attached to the carrier particles (i.e. carrier residue).

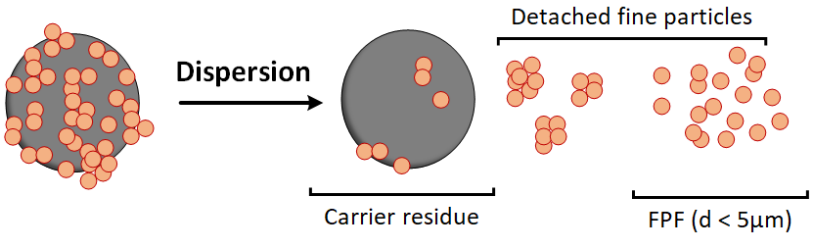

Figure 1.3: The concept of fine particle fraction (FPF) and other dispersion performance indicators [50].

1.3 Problem statement

The overall performance of a DPI relies on three factors: the formulation it contains, the design of the inhaler, and the patient's respiratory maneuver [45], and over the past few decades, overwhelming effort has been put into explaining performance with respect to these factors. These investigations primarily contribute to an understanding of the adhesive mixing for carrier-based DPI formulation and to linking the formulation variables to the *in vitro* delivered FPF value. The principal formulation variables that have been studied are:

- The geometrical attributes of (mainly) carrier particles, including size distribution, shape, and roughness [102, 44, 30, 31, 68, 78, 33].
- The physico-chemical properties of mixing components, including particles material, grade, and surface energy [105, 69, 75, 75].
- The formulation conditions, including mixing time, mixing intensity, loading ratio, press-on force, and relative humidity [73, 134, 67, 106, 135].
- The inclusion of fine excipient particles (i.e. **fines**) as the third component to the formulation [66].

From the dispersion perspective, the continuous attempt to develop formulation- and patient-independent drug delivery systems has brought several generations of inhalers into existence [25]. The key element of these developments is to maintain balance between the adhesion forces within the mixture components and the separation forces generated by the kinetic energy of the inhaled airstream.

Despite all the recent advancements in the formulation and dispersion of carrier-based DPIs, their detailed performance is not fully understood. A comprehensive work published by Hoppentocht et al. [60] in 2014, proceeded with an update in 2017 [25] shows that the *in vitro* delivered fine particle doses of currently marketed DPIs are at best less than 50% of their nominal values. This poor performance can be attributed to the following shortcomings in the basic understanding of DPI design:

1. **Lack of mechanistic understanding of the adhesive mixing process.**
   A major portion of studies on the relation between formulation variables and dispersion performance have overlooked the process of adhesive mixing. Evaluations of the formulation process, independent of dispersion tests, has largely been limited to a crude homogeneity assessment based on the relative standard deviation (RSD) of mixture composition. The RSD fails to provide detailed information on the structure of API particles over the carriers and the adhesive properties of the particle contacts.

2. **Inevitable interplay of principal variables in the formulation process.**
   Certain properties of particles involved in DPI formulation are difficult to quantify properly, and can rarely be changed in isolation from one another. For instance, the shape, roughness, and surface energy of carrier particles are closely intertwined, and therefore, it is a great challenge if not impossible, to single out a particular variable for further investigation.

3. **Conflict in findings related to the dispersion performance of DPIs.**
   Owing to the complexity of the formulation and dispersion process, some results of *in vitro* dispersion tests are inconsistent throughout the literature. A striking example is the role of carrier particle roughness on drug release during inhalation, wherein both direct [78] and inverse correlation [44] between roughness length-scale and FPF value have been reported.

A possible and common remedy for these challenges is to invest in developing a modelling framework for adhesive mixing and the aerosolization process, because such modelling makes a dynamic and detailed description of the mixing process available, with a spatial and temporal resolution of particle length-scale and inter-particle collision rate. So far, only a few preliminary and quantitative models have been proposed to link the microscopic features of adhesive mixing (or similarly dry-coating) and particle interactions in the system [3, 4, 59, 15, 114].
Existing studies based on particle dynamic simulation have also addressed the primary steps in the adhesive mixing process, including single agglomerate breakage at impact [118, 101, 117, 47], the adhesion of drug particle to a single carrier [96, 97], and the redistribution of drug particles over carriers [98]. The de-agglomeration mechanisms in an inhaler have also been scrutinized through micro-scale simulation of dispersion due to air flow [132], as well as particle-wall collision [121, 20, 120, 109, 122, 124].
However, the difficulties in simulating a large number of disparate-sized particles that are irregular and cohesive have impeded progress in this field. It is deemed necessary to have a model that encompasses all the stages of the adhesive mixing process, and it is crucial to determine the effect of influential parameters on the process behavior.

1.4 Objectives and thesis outline

The central objective of the present research is to establish a modelling framework for adhesive mixing and the dispersion of drug particles, in which the experimental concerns receive sufficient considerations. A substantial portion of this work is to:

- provide a mechanistic understanding of the adhesive mixing process by developing a novel modelling framework.
- design a methodology to assess the quality of adhesive mixing and dispersion process.
- unravel the effect of formulation variables on mixture quality and dispersion performance.

The present thesis is mapped out according to the objectives of the research and is divided into the following chapters. Chapter 2 elaborates on the theoretical concepts in adhesive mixing, along with the fundamental aspects of the computational framework. In Chapter 3, the simulation set up and the post-processing techniques are demonstrated. The main results of this research are reported and discussed in Chapter 4. Chapter 5 summarizes the important findings of the work and presents future opportunities for studies of the DPI formulation and dispersion processes. Finally, the outcome of the research is attached as Paper I to V.

2

Theory

This chapter presents some of the most fundamental concepts in the adhesive mixing process that are pre-requisite for grasping the principal variables in carrier-based DPI formulation. In addition, the components of the computational model are described in detail.

2.1 Randomized and ordered mixing

It is well established that binary particle mixing is theoretically controlled by two limiting cases:

1. For relatively coarse, free-flowing, and mono-dispersed particles, the *randomization* process governs the degree of homogeneity. This means that the probability of finding either of the mixing components is the same for any random sample that is withdrawn from the mixture.

2. If one particle exists in a fine or otherwise cohesive form, the particulate mixture shifts from randomized disorder to an *ordered* structure. This leads to the formation of coarse-fine ordered units, wherein the coverage ratio of ordered units, in the limit, is the same throughout the entire system (Fig. 2.1).

While the degree of homogeneity of ordered mixtures is theoretically calculated to be higher than that of a randomized mixture, it is doubtful if either of these ideal mixing states will ever be practically achieved. The deviation from these states is normally measured based on the statistical variation of composition among samples drawn from the mixture. The sample composition variance helps to quantify the degree of mixing by defining the mixing index as the ratio of "how much mixing has occurred" to "how much mixing can occur" [74]. This concept will be utilized to assess the quality of adhesive mixing for DPI formulation.

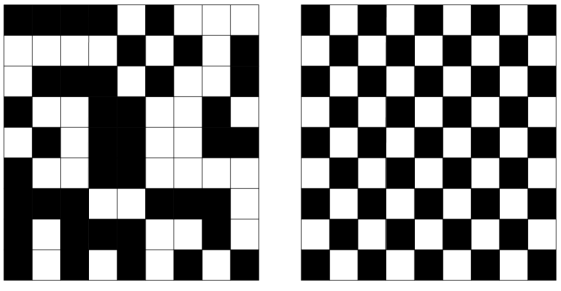

Figure 2.1: Distribution of black and white components in two ideal mixing states: (Left) Randomized binary mixture; (Right) Ordered binary mixture [56]

2.2 Cohesive-adhesive balance (CAB)

Assuming that enough mechanical energy is imparted to the assembly of drug and carrier particles, fragmentation of agglomerates occurs, and the API particles are made available to occupy carrier surfaces. The sufficiency of this energy is determined partly by the degree of *cohesion* among API particles, which controls agglomerate strength, and partly by the degree of *adhesion* between drug and carrier particles, which governs the formation of adhesive units. Therefore, a balance between the cohesive and adhesive behavior of particles is needed for the optimal performance of adhesive particle mixing.
The cohesive-adhesive balance (CAB) has been formulated as the ratio of the pull-off forces of drug-carrier to drug-drug particles [11]. A CAB ratio lower than 1 indicates the alacrity of drug particles and a CAB ratio higher than 1 indicates the reluctance of drug particles to interact with carriers. The key element of the CAB ratio is the pull-off force of two particles. This force may be attributed to multiple factors, including surface energy, relative humidity, the presence of ternary components, and the morphology of the carriers. In order to identify pull-off forces better, a brief explanation of inter-particle forces is presented here.

2.3 Inter-particle forces

Inter-particle forces can originate from several sources, including van der Waals forces, capillary forces, electrostatic forces, sintering, or chemical bonding. The presence of these forces and their relative dominance can tremendously alter the bulk behavior of particles, e.g. flowability or packing. The dominance of attractive forces is decided by their relative magnitude to particle weight, also known as the cohesive granular Bond number, Bo_g. This ratio serves to divide granular materials into two major groups: cohesive if the $Bo_g > 1$ and non-cohesive if the $Bo_g < 1$ [14]. Under dry conditions and complete dissipation of the build-up of electrostatic charges from interacting surfaces, the principal forces that govern the particle adhesion are of the van der Waals type.
Van der Waals force is a collective term that describes several long-range forces arising from permanent dipole/dipole interactions (Keesom) [70], permanent dipole/induced dipole (Debye), and London dispersion forces between molecules [63]. Van der Waals forces are one of the most common sources of adhesion as they are ever-present. Although fundamental theories to obtain these forces have been developed for molecular (or atomic) interactions, they can be adopted to calculate the interaction forces between macroscopic bodies, e.g. particles. Dispersion interactions are, at a first approximation, additive and non-retarded, and their contribution to the interaction energy between two macroscopic bodies can be obtained by integrating their effect over all pairs of atoms and the volume of objects. This integration is thus geometry-dependent and the resultant expression is generally described in terms of the Hamaker coefficient, A_H, [55] and characteristic lengths of bodies. For two flat surfaces in macroscopic contact, the van der Waals interaction energy per unit area is given as:

$$W = -\frac{A_H}{12\pi {z_0}^2} \tag{2.1}$$

where z_0 is the minimum separation distance, i.e. the equilibrium point between the attractive and the repulsive components of the van der Waals force.
According to the contact theory for granular materials [57], when two solid spheres of

radii R_i and R_j come into contact, the contact region is locally flat, and therefore, its corresponding adhesion force should be derived based on Eq. (2.1). As a result, the net adhesion force of two incompressible macroscopic spheres is governed by:

$$F_{sphere} = 2\pi\Big(\frac{R_i R_j}{R_i + R_j}\Big)W_{flat\ surface} \tag{2.2}$$

This formulation is known as the Derjaguin approximation [27] and is valid as long as the range of the interaction and z_0 are much less than the radii of the spheres. The interaction energy per unit area of flat surfaces is equivalently called the work of adhesion, and in a general form it takes the subscript of *132*, denoting the work of adhesion between surfaces 1 and 2, which interact in a third medium.
It is important to note that real particles, however, are never completely rigid, and they deform elastically under the influence of an externally applied load or the attracting forces that pull two surfaces together. In the latter case, the Derjaguin approximation should be refined in accordance with the contact mechanism to calculate the contact area and the adhesion force of the two surfaces.

2.4 Computational granular dynamics

Decades of scientific endeavor to understand the intricate behavior of granular materials have shown that an efficient approach to cope with the complexity of these materials is to model the motion of particles according to fundamental physical and mathematical principles. The advantages of mathematical modeling over experimentation are the detailed level of information modeling can provide as well as its relative cheapness and quickness. Different modeling approaches must be considered depending on the length and time scales of phenomena associated with particles. Generally, the existing approaches to modelling granular materials can be classified into two categories: the continuum approach at the macroscopic level and the discrete approach at the microscopic level.
The principle of continuum modelling is to consider particle flow as a fluid and solve the underlying conservation equations using Computational Fluid Dynamic (CFD) techniques. The level of detail of a flow description relies on the averaging technique and the closure model being applied to the continuum modeling framework. This approach overlooks the behavior of individual particles, and, for this reason, it is more preferred in process modeling containing a vast number of particles because of its computational convenience. A detailed description of the continuum modeling framework can be found elsewhere [48].
The discrete approach to simulating particle flow, also known as the Lagrangian particle method, essentially tracks the motion of individual particles with a numerical solution of translational or/and rotational equations of motion. There are a variety of discrete simulation methods that not only share many features but also have important differences in their formulation. The differences arise from the characteristic time and length scales of each method (see Fig. 2.2 [76]). The following section presents a brief description of one of the most prominent discrete models for the flow of granular materials used in the present work, namely the Discrete Element Method (DEM), along with its formulations.

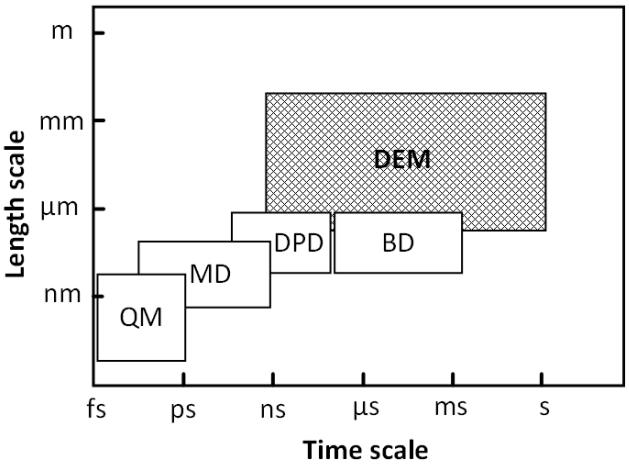

Figure 2.2: Schematic illustration of discrete modelling approaches at different time and length scales, including Quantum Mechanics (QM), Molecular Dynamics (MD), Dissipative Particle Dynamic (DPD), Brownian Dynamic (BD), and the Discrete Element Method (DEM) [76].

2.4.1 DEM governing equations

The DEM bears a resemblance to Molecular Dynamics [43], with the inclusion of a rotational equation of motion in the governing equations [23]. In this method, the following linear and angular momentum equations for the ith particle touching the j^{th} particle are solved. Consequently, an iterative time integration of the equations gives particle velocity and position.

$$m_i \frac{d\mathbf{v}_i}{dt} = \mathbf{F}_{ij}^{contact} + \mathbf{F}_i^{fluid} + \mathbf{F}_i^{body} \tag{2.3}$$

$$I_i \frac{d\omega_i}{dt} = \sum \mathbf{T}_i^{contact} + \mathbf{T}_i^{fluid} \tag{2.4}$$

DEM modeling has two different approaches for handling particle-particle collisions, referred to as the hard-sphere model and the soft-sphere model. Within the framework of the hard-sphere model, particles are assumed to be perfectly rigid, with collision among particles being instantaneous. Due to the rigidity of the particles' interaction, an event-driven algorithm can be used for simulation. Although the underlying assumptions of the hard-sphere model seem unrealistic, and the details of contact among particles are ignored, the model is valid when binary collisions dominate, and multi-particle contacts are rare. In contrast to the hard-sphere model, the soft-sphere formulation accounts for multibody and enduring contacts between particles. Based on this formulation, the magnitude of contact force is obtained from the contact area and can be a function of particle overlap, relative velocity, and contact history. The net contact traction distribution over this area can be decomposed into two orthogonal parts: a component normal to the plane (normal force) and a component in the contact plane (tangential force). Based on these features, the soft-sphere model is used in the present study.

2.4.2 Contact model

In the present work, the effect of interstitial flow on particulate behavior is inferred to be negligible based on an analysis of the Bagnold number [8]. This number is used to measure the importance of particle collisions on stress transmission and can loosely be interpreted as a ratio of the order of magnitude of particle collision stress to that of viscous fluid stresses in the flow field.
In the absence of particle-fluid interaction, the accuracy and realism of DEM simulation strongly depends on the contact model and its implementation. DEM contact models normally consist of a selection of springs, sliders, and dash-pots to represent the stress in a contact zone. It is essential to choose a contact model that matches the intrinsic degree of elasticity and cohesion of contiguous particles. The following is a description of the contact models relevant in the context of dry coating. A more detailed listing of available contact models, with both normal and tangential components, has been compiled by Morrissey [95].

2.4.2.1 Elastic interaction: Hertz-Mindlin model

The most common formulation used to calculate the normal and tangential force vs. displacement relationships for elastic spheres with friction are provided by the theories of Hertz [57], Mindlin [90], and Mindlin and Deresiewicz [91]. According to the Hertz theory, when two elastic spheres of radii R_i and R_j come in contact, a semi-ellipsoidal stress distribution is created over the circular contact area (see Fig. 2.3).

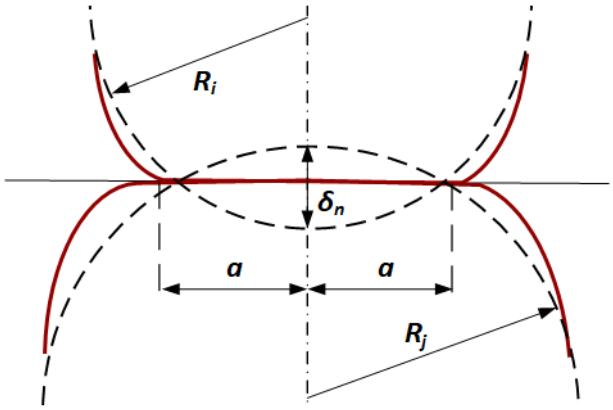

Figure 2.3: Geometry of local deformation in the contact area between two similar, unequal-sized elastic spheres based on the Hertz theory (vertical scale is exaggerated). Solid curves represent the realistic behavior of two particles in contact, while dashed curves represent the artificial penetration of two particles.

For the contact area with radius a, the stress distribution is given by the following expression:

$$p(r) = p_0 \left[1 - \left(\frac{r}{a}\right)^2\right]^{\frac{1}{2}} \tag{2.5}$$

where p_0 is the maximum pressure corresponded to the center of the contact area. This

parameter is linked to the contact radius as:

$$a = \frac{\pi p_0 R^*}{2E^*} \tag{2.6}$$

The total normal force can be calculated by integrating the distribution over the contact area:

$$F_{ne} = \int_0^a p(r) 2\pi r dr = \frac{2}{3} a^2 \pi p_0 \tag{2.7}$$

Using the geometrical relationship for non-adhesive contact, the radius of the contact area is correlated to the relative normal displacement of particles, δ_a, as:

$$a^2 = R^* \delta_n \tag{2.8}$$

The normal force-displacement relationship can be obtained from the following nonlinear expression:

$$F_{ne} = \frac{4}{3} E^* \sqrt{R^* \delta_n^3} \tag{2.9}$$

from which the normal contact stiffness is defined as:

$$k_n = \frac{\mathrm{d}F_{ne}}{\mathrm{d}\delta_n} = 2E^* \sqrt{R^* \delta_n} \tag{2.10}$$

The effective Young modulus E^* and the effective radius R^* are defined as:

$$\frac{1}{E^*} = \frac{(1-\nu_i^2)}{E_i} + \frac{(1-\nu_j^2)}{E_j} \tag{2.11}$$

$$\frac{1}{R^*} = \frac{1}{R_i} + \frac{1}{R_j} \tag{2.12}$$

The simplest non-linear model in the tangential direction in the DEM simulations is the elastic solution proposed by Mindlin [90] for no-slip contacts under a constant normal force of F_n. The component is given as:

$$F_t = 8E^* \sqrt{R^* \delta_n} \delta_t \tag{2.13}$$

or in terms of tangential contact stiffness:

$$F_{te} = k_{t0} \delta_t \tag{2.14}$$

The term slip in this theory describes the small relative tangential motion over part of the contact area caused by applying a tangential force of $F_t < \mu F_n$. By this definition, a complete no-slip condition is improbable in an incremental loading of two particles. The possible micro-slip effect justifies the inclusion of a dissipation term in the Mindlin model. This modification was done by Mindlin and Deresiewicz [91], and it implies that the general force-displacement relation depends on the whole loading history and on the instantaneous rate of change in the normal and tangential force or displacement. The Mindlin and Deresiewicz model gives a subtle function of tangential contact stiffness k_t against tangential displacement for loading, unloading, and reloading conditions. Figure 2.4 presents a schematic diagram of the tangential force-displacement proposed by Mindlin and Deresiewicz [125, 29].

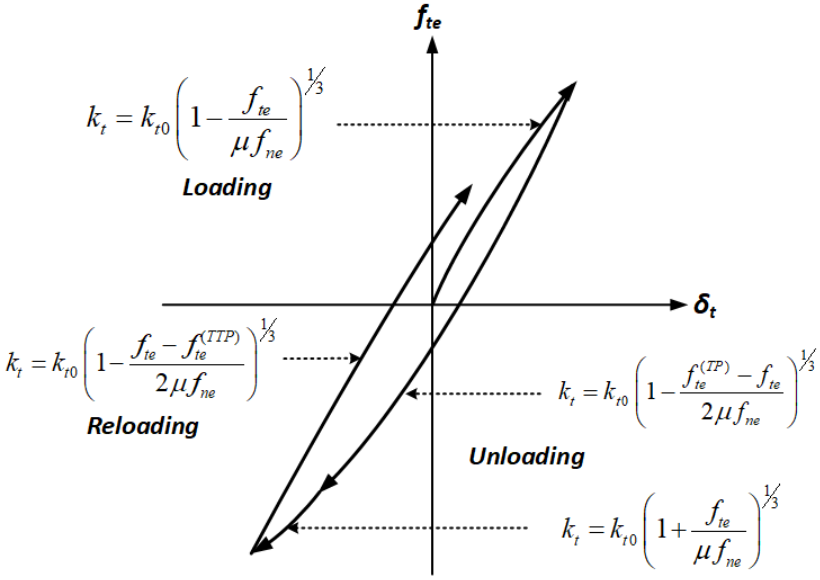

Figure 2.4: Tangential force-displacement for loading, unloading, and reloading under constant normal displacement. (TP) and (TTP) indicate the first and second turning points in the tangential force, respectively [29].

2.4.2.2 Adhesive elastic interaction: Johnson-Kendall-Roberts model

To calculate the elastic contact force in the presence of van der Waals adhesion, the classic Hertz model must be modified. The most common approaches for handling adhesive contact are based on the JKR [65] and DMT [28] theories. In the JKR model, the contact is considered to be adhesive, and, therefore, the contact area is correlated to elastic material properties plus the interfacial interaction strength. Due to the adhesive contact, contacts can be formed during the unloading cycle also in the negative loading (pulling) regime. On the other hand, the DMT theory considers van der Waals interactions outside the elastic contact regime and increases the particle load. In general, the DMT theory is used for small and stiff particles and the JKR theory for large and compliant particles. The Tabor number [111], μ, which gives a measure of the extent to which adhesive forces are capable of deforming a particle, can be used to identify the interaction regime with the criterion that for $\mu < 1$, the DMT theory should be used, and for $\mu > 1$, the JKR theory should be used. This number is defined as:

$$\mu = \left(\frac{R^*\Gamma^2}{E^{*2}{z_0}^2}\right)^{\frac{1}{3}} \tag{2.15}$$

These two models represent opposite extremes of one scale for adhesive contact behaviour, as described by Maugis [88], and the transition between them can be predicted more accurately from the dimensionless parameter of λ defined as:

$$\lambda = 2.06\left(\frac{R^*\Gamma^2}{\pi E^{*2}{z_0}^3}\right)^{\frac{1}{3}} \tag{2.16}$$

where JKR applies if $\lambda > 5$ and DMT applies if $\lambda < 0.1$. This criterion is recommended over the Tabor number, as the latter one is argued to sometimes lead to a poor choice of adhesive model [32].

Based on the above criteria, the JKR model was chosen as the primary normal contact model in the present study. For this reason, the JKR model will be the focus of the following discussion. According to this theory, the radius of the contact region is dependent on the normal-elastic force and the interface energy between both particles as follows:

$$a^3 = \frac{3R^*}{4E^*}\Big(F_{ne} + 3\pi\Gamma R^* + \sqrt{6\pi\Gamma R^* F_{ne} + (3\pi\Gamma R^*)^2}\Big) \tag{2.17}$$

where only the positive root is allowed for stable equilibrium. According to the force-contact area relationship of the JKR interaction, in the loading regime and compared to the common Hertzian contact model, Eq. (2.17) generates a larger contact area due to the attractive interaction. As a result of this attraction, a finite contact area will exist even under zero external load (equilibrium contact area) with the radius of:

$$a_0^3 = \frac{9\pi\Gamma R^{*2}}{2E^*} \tag{2.18}$$

Furthermore, contacts in the JKR model can endure the unloading regime up to negative overlap values because of particle necking. The maximum tensile force required to break the contact is called the pull-off force and is expressed as:

$$F_C = \frac{3}{2}\pi\Gamma R^* \tag{2.19}$$

and its corresponding overlap is:

$$\delta_C = \frac{a_0^2}{2(6)^{\frac{1}{3}}R^*} \tag{2.20}$$

From computational point of view, having critical force and overlap as well as normal overlap can lead to the calculation of contact radius and, eventually, the normal elastic force. The procedure for this calculation is based on the following expressions [18]

$$\frac{\delta_N}{\delta_C} = 6^{\frac{1}{3}}\Big[2(\frac{a}{a_0})^2 - \frac{3}{4}(\frac{a}{a_0})^{\frac{1}{2}}\Big] \tag{2.21}$$

$$\frac{F_{ne}}{F_C} = 4(\frac{a}{a_0})^3 - 4(\frac{a}{a_0})^{\frac{3}{2}} \tag{2.22}$$

The solution to the governing non-linear equation with respect to the dimensionless overlap is shown in Fig. 2.5. The normal-elastic force is defined as positive while particles push toward each other. As they move away from each other, the normal force becomes negative, and the particle normal overlap begins to decrease. However, the particles remain in touch due to cohesion, even at a negative value of δ_n, via necking of the material. This attachment continues until the critical point, where $\delta_n = -\delta_C$ [87].

It is necessary to unify one concept that appears with different notation in the literature. In the original article by Johnson, Kendall, and Roberts [65], the interfacial energy of particles (Γ) is addressed as energy per unit contact area (γ), and, according to Israelachvili [63], this is the same as the work of adhesion (W). For particles of dissimilar materials, a good approximation is to use the combining law of the particle work of adhesion as follows:

$$W_{ij} \approx \sqrt{W_{ii} \times W_{jj}} \tag{2.23}$$

This approach is used in the present study, and it is consistent with the general method of calculating the Hamaker constant of dissimilar interacting bodies [13]. From this approach,

the work of adhesion of two dissimilar particles will be slightly different than what is usually calculated using the well-known Dupré equation [35] [1].

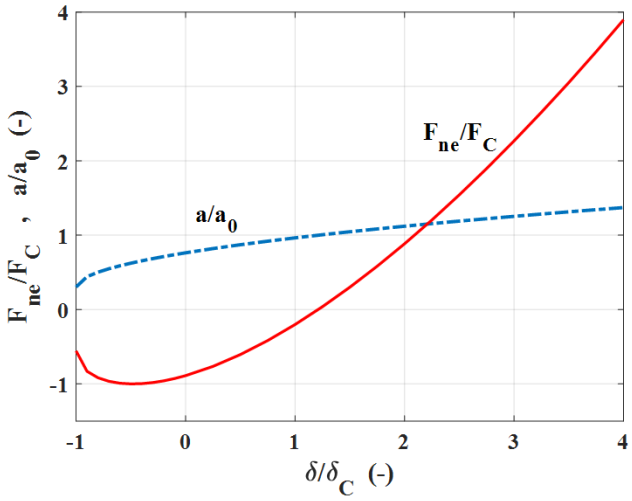

Figure 2.5: Dimensionless JKR adhesive elastic force and corresponding contact radius vs. particle overlap. According to the JKR theory, there is a finite contact area, even under zero load, due to particle auto-adhesion.

Similar to the normal component, the tangential component of contact force must be modified in the presence of van der Waals attractive forces. This modification is of great importance mainly in cases where an agglomerate is torn apart either by a fluid shear or collision with another agglomerate [116]. A simplified approach has been proposed by Thornton [115], wherein the micro-slip model of Mindlin and Deresiewicz is valid only if the tangential force exceeds a critical value of $F_{crit} = \mu_f |F_{ne} + 2F_C|$. For tangential forces below this critical value, a so-called peeling mechanism governs the behavior of particles in contact.

2.4.3 Viscous dissipation forces

In the context of soft-sphere modeling of quasi-static particulate systems, it is common to add a dash-pot to the spring assembly that describes the contact. The dash-pot forces are not considered to be part of the actual contact model, but they are added to account for the dissipation of energy caused by the elastic wave propagation through a solid particle. The dash-pot forces are a function of the displacement rate and are generally described as [126]:

$$F_n^d = \alpha(e)\sqrt{m^* k_n}\,\dot{\delta}_n = \alpha(e)\sqrt{m^* k_n}\,(\mathbf{v}\cdot\mathbf{n_{ij}}) \tag{2.24}$$

$$F_t^d = \alpha(e)\sqrt{m^* k_t}\,\dot{\delta}_t = \alpha(e)\sqrt{m^* k_t}\,(\mathbf{v}\cdot\mathbf{t_{ij}}) \tag{2.25}$$

where $\alpha(e)$ is a function of the restitution coefficient, which was initially determined by Tsuji et al. [123] through numerical calculation. An analytical expression for $\alpha(e)$ was derived by mapping the Hertz-based contact model to the Hooke-based contact model [6],

[1] Israelachvili, personal communication 2017

which resulted in the following expression:

$$\alpha(e) = \frac{-\sqrt{5}\ \ln(e)}{\sqrt{\ln^2(e) + \pi^2}} \tag{2.26}$$

Throughout this study, a viscous term was added to both the normal and tangential components of the model to account for the dissipation of energy in the contact.

2.4.4 Rolling resistance

The net tangential force that acts on each particle can be utilized to calculate the rolling torque of the particle. In addition to this torque, there is a friction torque caused by the rolling resistance between particles, which is mainly a function of the relative angular velocities (ω_{rel}) of the particles. A direct constant torque model proposed by Zhou et al. [139] was used to assess the value of the rolling resistance moment ($\mathbf{M}_r$) as follows:

$$\mathbf{M}_r = -\frac{\omega_{rel}}{|\omega_{rel}|}\mu_r R^* F_{ne} \tag{2.27}$$

$$\omega_{rel} = \omega_i - \omega_j \tag{2.28}$$

where μ_r is the rolling friction coefficient and depends on the type of particles that are in contact. This model is considered to be the simplest model for assessing rolling resistance that is computationally adequate and accurate for particle assemblies with a low rolling friction coefficient [140, 141]. Detailed information about rolling resistance and the different models available for calculating resistance can be found in [1].
It has been discussed by Marshall [87] that the van der Waals adhesion force imposes an asymmetry on the contact region, and therefore, an additional rolling mechanism needs to be included in the above formulation. An efficient numerical implementation of this mechanism into the contact model has been proposed by Eidevåg et al. [38], wherein the rolling coefficient is determined by the particle adhesion hysteresis.

2.4.5 Time stepping in DEM

It is noteworthy that a key factor of the stability and precision of DEM simulations is the time step. During its movement, a particle may collide with neighboring particles or walls. However, a particle's movement is also affected by particles far beyond its local neighborhood through the propagation of disturbance waves. This problem is solved by selecting a suitably small value for the time-step such that, during a single time-step, a disturbance can only propagate from one particle to other particles in contact with it. For non-linear contact models, such as JKR, the critical time-step cannot be calculated a priori, instead it can be estimated using the Rayleigh wave speed [89]. According to Thornton [116], the proper time step can be chosen as a fraction ($\approx 20\%$) of the Rayleigh critical time step (Δt_c) for the smallest particle in the system, which is calculated using the following expression:

$$\Delta t_c = \frac{\pi R_{min}}{0.8766 + 0.1631\nu}\sqrt{\frac{\rho}{G}} \tag{2.29}$$

2.4.6 Simulation of non-spherical particles

A challenge in simulating particulate systems is representing complex-shaped particles because of the profound effect of particle geometry on the static (e.g. packing) and dynamic (e.g. flow) behavior of such systems [82, 19]. In order to incorporate particle shape and roughness into the simulation framework, two challenges must be met. One is to mathematically define the particle shape and roughness, and another is to make this mathematical definition compatible with the existing numerical scheme. These challenges are addressed here.

2.4.6.1 Particle shape quantification

A preliminary step to build up a realistic non-spherical particle is to get the mathematical description of its shape, generally referred to as shape characterization. This step has two main phases: initially, the particle shape is assessed using imaging or scanning techniques, and, later, the shape is transformed into quantitative morphological and textural descriptors [10] using image processing algorithms such as segmentation algorithms [129]. Typically, the particle shape is characterized using elongation, flatness, sphericity, or roundness, among other parameters.
An alternative approach to quantify particle shape is to use the closed-form Fourier function initially introduced by Ehrlich and Weinberg [37]. In this approach, the 2D profile of a particle, or any arbitrary cross-sectional image of a 3D particle (Figure 2.6), is mathematically described with the following series:

$$r_i(\theta_i) = r_0 + \sum_{n=1}^{N} \Big[(A_n \cos(n\theta_i) + B_n \sin(n\theta_i) \Big] \tag{2.30}$$

where r_0 is the average radius, N is the total number of Fourier harmonics, n is the harmonic number, and A_n and B_n are the coefficients for magnitude and phase, respectively, for each harmonic. The normalized Fourier descriptor of each harmonic, D_n, is then calculated based on the latter coefficients as:

$$D_n = \frac{\sqrt{A_n^2 + B_n^2}}{r_0} \tag{2.31}$$

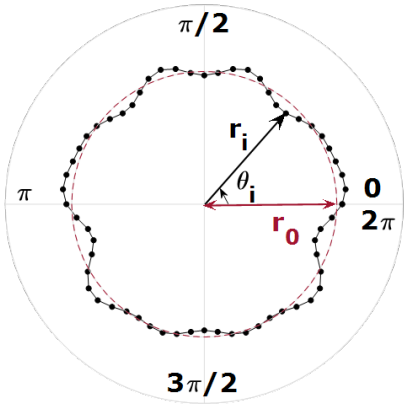

Figure 2.6: The polar representation of a non-spherical particle profile.

The Fourier descriptors are experimentally measured by scanning or imaging a particle, then discretizing the image to assess the surface profile of the particle, and finally by

applying the Fourier transform. A novel idea, introduced by Mollon and Zhao [92, 93], was to reverse this concept, namely, by performing an inverse Fourier transform on a given spectrum as the starting point for generating particles with prescribed shape features. To perform this task in 3D, a mathematical procedure based on random field theory has been adapted. Any arbitrary point on the external surface of a particle with controlled shape features is expressed as $P_i = (r_i, \theta_i, \phi_i)$, wherein r can be regarded as a random field defined on a spherical domain. Moreover, the relative position of any pair of points (P_i, P_j) can be determined by using the autocorrelation function between the pair-point variables of r_i and r_j. Fortunately, the theory of signal processing provides a direct relation between this required autocorrelation function and the given Fourier spectrum. Therefore, all the points on the external surface of a particle can be assessed by assigning an initial random point and the corresponding Fourier spectrum. The outcome of this model is a 3D convex-hull, including the vertices and faces that portray the particle.

2.4.6.2 Representing non-spherical particle for DEM

A practical obstacle after creating the particle 3D convex-hull is to implement it into the framework of a particulate simulator, i.e. a DEM. This challenge arises from the fundamental assumption of many available simulation packages, which is to perceive particles as smooth spherical elements. One salient solution to this problem is to capture the particle shape by inscribing overlapping spheres of different radii within the shape outline. This solution was first proposed by Favier et al. [41] and is referred to as the multisphere model. The multisphere model overcomes all the intricacies of detecting a contact plane and calculating the particle overlaps that are present in other non-spherical DEM schemes (e.g. using ellipsoids [119, 77, 36], superquadric functions [128, 127, 81], polyhedral shapes [22, 46], or the NURBS technique [5]). The internal contacts between spherical elements are ignored in this model, and the entire particle is treated as a rigid body.

The mathematical algorithm to achieve a multisphere model of the 3D convex-hull is commonly known as an overlapping discrete element cluster (ODEC) [7]. In recent years, this class of algorithms has been enhanced to become faster, more efficient, and more importantly, to handle the induced non-uniform density inside a particle. The 3D ODEC algorithm proposed by Ferellec and McDowell [42] was selected as the basis of the present study. In this algorithm, an arbitrary point is chosen on the surface of the particle, then a sphere is grown along its internal normal direction and expands until it reaches another point on the surface of the particle. This procedure continues until there is one sphere for each point. The gap between surface nodes, the minimum radius of the spheres, and the maximum number of spherical elements control the accuracy of the shape approximation with this algorithm.

2.5 Particle roughness

Besides shape, the surface roughness of a carrier particle in DPI formulation has been found to have a dominating effect on drug dispersion, and therefore it is well worth pondering. The roughness of a particle can be analyzed according to the principles of conventional methods by which the roughness of a solid flat surface can be determined. In the classical approach, the surface is scanned with various contact/noncontact techniques until the surface profile has been extracted [12]. This profile contains a range of spatial amplitudes and frequencies that provide morphological information on the surface. The amplitudes

of the surface profile demonstrate peak-to-valley distances and are normally reported in terms of statistical parameters that show deviation from the surface reference line.
Over a sampling length of L, the surface profile consists of M measurements on the profile height in the form of $z_i(x_i)$. The average roughness (R_a) and the root-mean-square (rms) roughness are the most commonly employed parameters used to describe roughness and are defined as [9]:

$$R_a = \frac{1}{L}\int_0^L |z(x)|\, dx \tag{2.32}$$

$$rms = \sqrt{\frac{1}{L}\int_0^L z(x)^2 dx} \tag{2.33}$$

2.5.1 Rough particles in contact

As engineered surfaces are nominally flat, a proper contact model needs to consider surface asperities. Experimental observations have revealed that the real contact area for particle interaction, in the presence of roughness, is less than 15% of the apparent contact area that is estimated from particle size and physical properties [40]. The contact between two surfaces, of which at least one has small corrugations, occurs at a myriad of discrete micro-contact points. One of the classical approaches to incorporating surface roughness into the contact mechanism is named after Greenwood and Williamson (GW) [53]. In this approach, a statistical model is proposed to describe surface roughness, and by combining this model with the Hertzian elastic theory, a solution to the contact problem of rough surfaces is derived. The GW approach is founded on the assumptions that the summit of each asperity is spherical with a constant curvature that deforms separately under load, and the height profile of asperities have a Gaussian distribution.
An alternative to this indirect approach and other indirect solutions to rough surfaces in contact (e.g. the fractal model by Majudamer and Bhushan [86]), is to approximate the micro-scale nature of the rough surface and directly resolve the contact model for each individual asperity of the surface. This approach relies, firstly, on the mathematical definition of the surface roughness, and secondly, on the method to make this definition compatible with the simulation environment. . A characterization technique based on the Fourier transform of the surface profile is employed to govern the mathematical definition of a surface. Thereafter, an algorithm for clustering the spherical elements is applied to create irregular particles with micro-scale roughness (Figure 2.7).

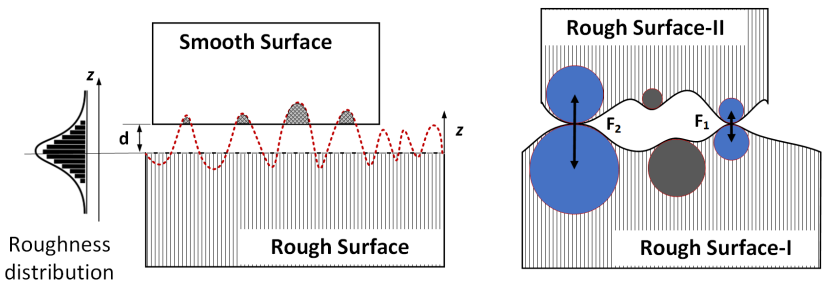

Figure 2.7: (Left) Theoretical scheme of the Greenwood-Williamson model of a rough surface in contact with a smooth surface: (Right) approximating the microscale nature of rough surfaces with spherical elements in order to explicitly resolve the contact problem.

2.5.2 Adhesion force distribution on rough surfaces

While the adhesion force between rigid and smooth spheres in contact is approximated by Eq. (2.2), it needs further development to calculate the interaction force in the presence of roughness. An early modification was carried out by Rumpf [104], wherein the radius of a single asperity was incorporated into this formulation. Later, a more sophisticated model was developed by Rabinovich [103], which requires the measurement of roughness, including the rms and distance between asperities, in two different length scales.

Atomic force microscopy (AFM) measurements in association with these theoretical models provide globally-averaged values for adhesion force and the corresponding roughness attributes of rough particles. However, these quantities have experimentally been found to be strongly distributed, and therefore, referring to measurements for one particle and only one position on a heterogeneous surface may be misleading. Due to the morphological variations in the contact zone of adhesive partners, three types of adhesion force distributions have been experimentally identified for rough surfaces [54]:

- **Type I**: The Weibull distribution, which applies to the adhesion of relatively smooth particles to substrates with a narrow distribution of the asperity radius.

- **Type II**: The bimodal Weibull distribution, which describes the adhesion between particles and substrates with similar orders of magnitude of roughness.

- **Type III**: The log-normal distribution, which corresponds to surfaces with rather broad heterogeneity in asperity size distributions.

2.5.2.1 Surface activity of carrier particles in DPI

Adhesion force distribution is in accordance with the prevailing definition of carrier surface activity in adhesive mixing for inhalation. It is widely accepted that the carrier particle surface is overrun by a range of sites with varying extents of activity that can host a drug particle. However, there is not enough knowledge on what essentially constitutes an active site, or if the sites can be regarded as discrete locations. This definition has been improved by Grasmeijer et al. [51], as they inferred that the surface activity of a carrier is the ability of the carrier site to retain drug particles during dispersion. This means that not only the binding energy of drug-carrier but also the separation energy provided upon the dispersion process determine surface activity.
AFM measurements at multiple sites on the surface of different lactose particle samples have shown that the adhesion force exhibits Type III, i.e. log-normal distribution, which can be expressed by the geometric mean force and the geometric standard deviation [79]. An example of AFM data for a Pharmatose 325-M particle is shown in Fig. 2.8.

This innate non-uniformity of adhesion force is an essential element of the simulation model in order to investigate the relative competition of different mixing components to preferentially occupy more active sites. The significance of this model is explained in the context of ternary DPI formulation.

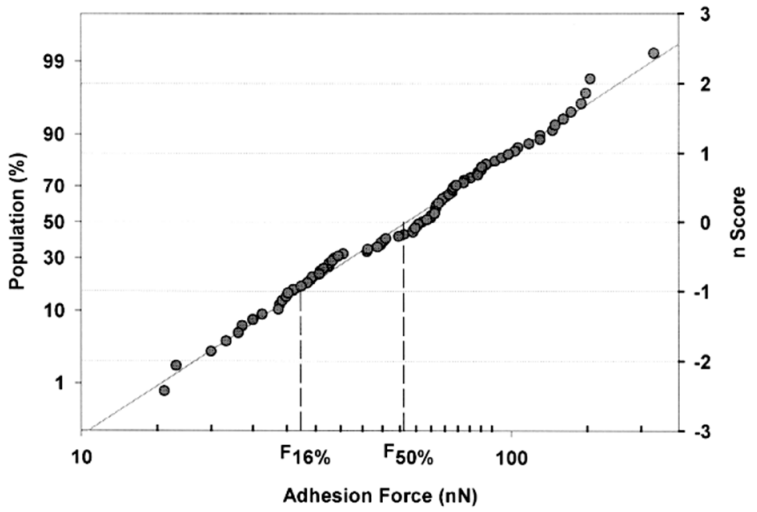

Figure 2.8: The adhesion force distribution of 325-M lactose particles shows that the data follows a log-normal distribution with a regression coefficient of 0.99 [79]. Reprinted with permission from Elsevier.

2.6 Fine excipient particles in DPI formulation

The performance of carrier-based DPIs can be significantly enhanced by the inclusion of a small amount of **fine** excipient particles into the binary blend of drug and carrier. Extensive research on the carrier-fine-drug ternary mixture has shown that fine excipient particles improve the performance of DPI formulation to varying extents depending on the excipient's material, the amount and size of the fine particles, and the blending sequence of mixture components [66].
An unsettled question on the contribution of fine excipient particles to DPI formulation is the underlying mechanisms by which the performance of a carrier-based ternary mixture increases. Several theories have been proposed in the literature to address this question:

1. **The active site theory** suggests that carrier surface activity has a heterogeneous distribution, and fine excipient particles compete with drug particles for high-energy binding sites. This competition forces the drug particles to interact with passive or low energy sites, which facilitates drug-carrier detachment [137, 136, 107].

2. **The agglomeration theory** focuses on the possible formation of fines-drug aggregates during blending. These agglomerates are subject to stronger aerodynamic drag forces during aerosolization than small drug particles, which results in a higher FPF [83, 84, 80].

3. **The fluidization reinforcement hypothesis** argues that the presence of fines increases the tensile strength of the powder bulk and, thereby, shifts the minimum fluidization velocity (MFV) in the inhalation chamber. This phenomenon intensifies inter-particle collisions and enhances the likelihood of drug-carrier de-agglomeration [108].

4. **The buffer hypothesis** states that fines act as a buffer between colliding carriers and protect drug particles from press-on forces. According to this theory, the fine particles aid dispersion only if the fine/drug particle size ratio is above one, as the sheltering effect depends on this size disparity [30].

While these mechanisms appear plausible, they remain somewhat speculative due to the abundance of experimental findings under similar conditions that support alternative choices. One shortcoming that leads to such discrepancies in the assessment of DPI performance is the lack of a mechanistic understanding of ternary mixing, and therefore, it is crucial to investigate formulation performance independent of the aerosolization process. The ability to impose non-uniform adhesion distribution to a carrier particle is a promising technique to determine the dominance of each mechanism, especially the active site theory. For example, the experimental supporting evidence of this theory was extracted by studying the effect of blending order of mixture components on formulation performance, as follows:

The FPF of a formulation prepared, first, by blending carrier and fines and then adding the drug has been found to be greater than a formulation prepared by adding fines after blending carrier and drug particles. It has been proposed that, in the first mixing scenario, fines have the advantage of establishing contact with more adhesive sites, while in the second scenario, the strong binding sites of the carrier are occupied by drug particles instead. As the powder is subjected to aerosolization, the first mixture releases more drug particles than the second mixture due to the relative strength of carrier-drug binding forces (see Fig. 2.9).

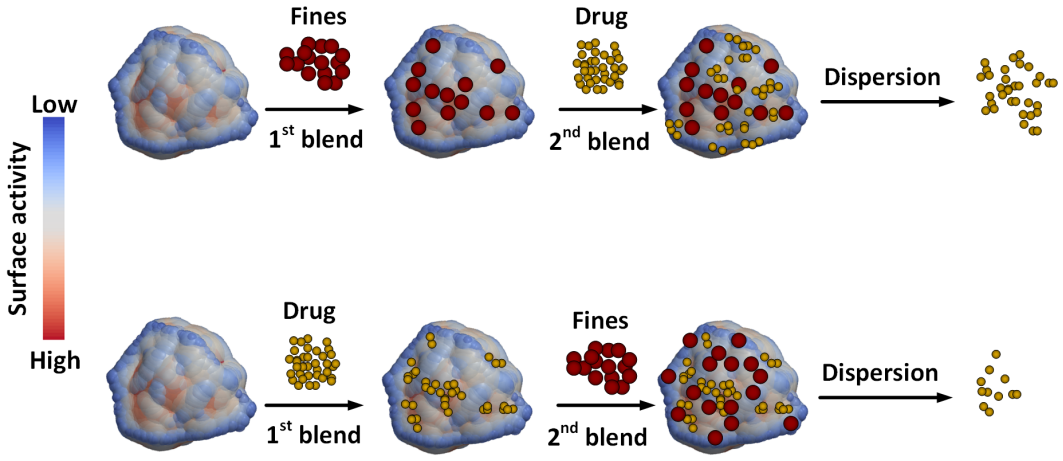

Figure 2.9: Speculated effect of blending order on final blend structure and the efficacy of dispersion process [66].

3
Simulation

The simulation set-up for the present study is elaborated in this chapter, and the chapter proceeds with the post-processing techniques.

3.1 Numerical implementation

A substantial part of the simulations was conducted in LIGGGHTS®, an open source software package for modelling granular materials developed by Kloss and Goniva [71]. It stands for LAMMPS Improved for General Granular and Granular Heat Transfer Simulations. LAMMPS is a classical simulator for MD, and it is widely used in this field. Its platform offers a `GRANULAR` package that can easily be adopted for DEM simulations. The default version of LIGGGHTS uses a somewhat simplified JKR model to handle adhesive contacts. The source code was modified in the present work to include the original JKR contact model. The remaining part of simulations was carried out using Altair EDEM® commercial software which is originally developed by DEM Solutions Ltd. The embedded Hertz-Mindlin with JKR v.2 model was selected as the contact model along with integrated modification of frictional force and rolling torque due to van der Waals adhesion.

3.2 Material selection

The DEM simulation requires the physical and mechanical properties of the mixing components. A majority of studies on adhesive mixing for inhalation have focused on the particulate materials that are most common in marketed formulations, including lactose and mannitol as carriers, salbutamol sulphate and budesonide as drugs, and lactose as fine particles [50].
Different combinations of these common particles were selected for the corresponding simulations in this work. Binary blends of D-mannitol carrier and lactose monohydrate as a placebo (a substitute for a drug), binary blends of lactose carrier and salbutamol sulphate as a model drug, and ternary blends of lactose carrier, lactose fines, and salbutamol sulphate as a model drug were studied.
It is worth mentioning that finding the necessary material properties for pharmaceutical particles can be an arduous, if not impossible, task. These data are sometimes reported to fall within a wide range of values (e.g. the Young modulus of lactose particles) or are often rare hard to find (e.g. the rolling friction coefficient for salbutamol sulphate). In such circumstances, an average or an approximate value based on similar materials found in the literature are used. These properties and their values are reported in detail in each paper.

3.3 Drug particle agglomeration

Since the natural cohesion of drug particles causes them to aggregate, it is essential to introduce these particles in the correct initial state into the simulation domain. In order to mimic drug agglomeration, the primary particles were randomly generated in a small confined space (spherical or cubical pseudo-region), then a small centripetal force was assigned to these particles, and the agglomerate started to form by the gradual cohesion between drug particles. Simulation continued until the initial kinetic energy was entirely dissipated, and the agglomerate reached steady state in size, void fraction, and coordinate number. The number of constituent particles in each agglomerate was flexible throughout the course of this study, ranging from 100 up to 5000, depending on the desired size of the agglomerate.

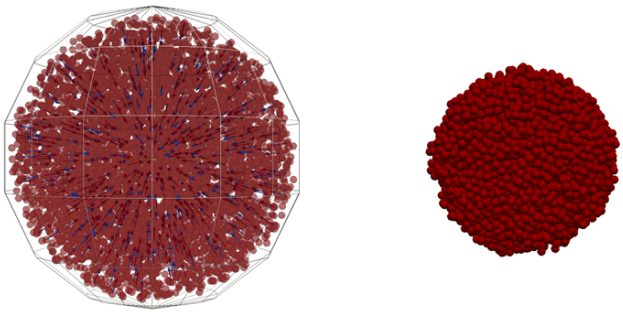

Figure 3.1: (Left) Initial state of particles before agglomeration; (Right) Final configuration of an agglomerate made of 5000 drug particles.

Table 3.1: Properties of the agglomerates used in the current study.

Agglomerate Properties	**No. I**	**No. II**	**No. III**
Primary particle size (μm)	5	5	3
Number of particles in agglomerate	5000	1000	100
Average size (μm)	115	60	20
Average packing fraction	0.4	0.4	0.35
Reference	Paper III	Papers I, II	Paper V

3.4 Selection of mixer

The industrial- and laboratory-scale powder blending for DPI formulation is carried out in both low-shear tumbling mixers (e.g. Turbula T2F) and high-shear mixers (e.g. Diosna). From the modelling perspective, however, it is more feasible to perform the blending under a high-intensity shear to save simulation time. Two different high-shear mixers were selected for the simulation of adhesive mixing in this study:

- a Couette shear cell, which has a well-known rheology and is capable of imposing constant and effective shear to particles [85, 61]. It poses a simple flow pattern mainly determined by carrier particles, with a near-constant shear rate and a non-vanishing velocity component in the θ direction.

- a vibrating cell, wherein a high-intensity vibration is induced in the cuboidal vessel that contains the particles. The cell oscillates at a preset amplitude and frequency along the z, y, and x directions. This three-dimensional vibration ensures that kinetic energy is properly transferred to all the particles, and thus, it accelerates the mixing process [131, 26].

3.5 Impact test

A primary step in the adhesive mixing process is the collision between drug agglomerates and carrier particles. This step, mostly in form of agglomerate-wall impact, were numerically simulated and carefully scrutinized in order to address the question of "How do agglomerates fracture?" [47]. These studies have provided comprehensive information on agglomerate breakage patterns and the principal parameters that affect breakage. These parameters are often lumped together to form a dimensionless collision number (Δ) that determines the behavior of an agglomerate at impact [94]:

$$\Delta = \frac{\rho D^{5/3} E^{2/3} V^2}{\Gamma^{5/3}} \tag{3.1}$$

This number demonstrates the ratio of incident kinetic energy to the internal resisting energy of the agglomerate against breakage. The impact test in the present work was performed by assigning a predetermined velocity to the agglomerate and having it collide with a fixed target particle. This configuration for a collision test helps to reveal not only the breakage of the drug agglomerate but also the adhesion of drug particles to the carrier surface. It also provides a chance to investigate the effect of target particle shape on the breakage and adhesion of the agglomerate upon impact.

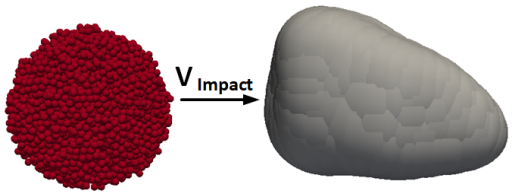

Figure 3.2: Configuration of an agglomerate and a target particle before impact test.

3.6 Dispersion test for an adhesive unit

A simplified and adequate assessment of the dispersion performance of a DPI formulation can be done by developing a purely DEM-based model for drug particle detachment from the carrier due to a wall collision.
In this work, a number of coated carrier particles were prepared for the wall-collision test in the following manner: After setting up a carrier particle, 2000 mono-sized drug particles were randomly generated in a pseudo-region in the form of a spherical shell around a carrier particle. These drug particles were slowly dragged towards the center of the carrier particle until contact was established, they adhered to its surface, and the initial kinetic energy

was entirely dissipated. This led to a stable drug-carrier adhesive unit. After the coating process was finished, the drug-carrier adhesive unit was forced to collide with a rigid wall in a normal direction at different impact velocities (see Fig. 3.3). Complementary work by Sommerfeld and Cui [21] signifies that the probability of the fluid dynamic detachment of a drug particle at these relative velocities is low, and the wall collision is the controlling mechanism for dispersion.

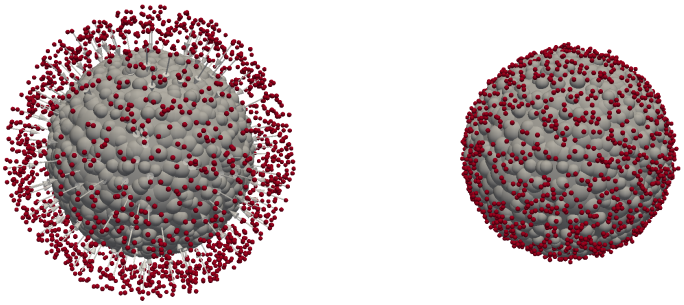

Figure 3.3: (Left) Initial state of particles to generate an adhesive unit; (Right) Final configuration of an adhesive unit with 1.6% drug particle and a coverage ratio of 20%.

3.7 Post-processing

3.7.1 Agglomerate fragmentation

To gain further insight into agglomerate fragmentation, a cluster detection method called Density-Based Spatial Clustering of Application with Noise (DBSCAN) [39], was used to detect fragments of agglomerates (sub-agglomerates) after breakage. This algorithm classifies primary particles into three groups based on their positions: core, border, and noise particles. Two parameters are necessary for this classification: a maximum acceptable distance between points (ϵ), and a minimum number of points in each cluster (MinPts). Figure 3.4 shows the principle of the DBSCAN algorithm, based on which a swarm of points were categorized. The MinPts was set at 5 in the present study, whereas the ϵ was chosen to be equal to the diameter of the fine particle.

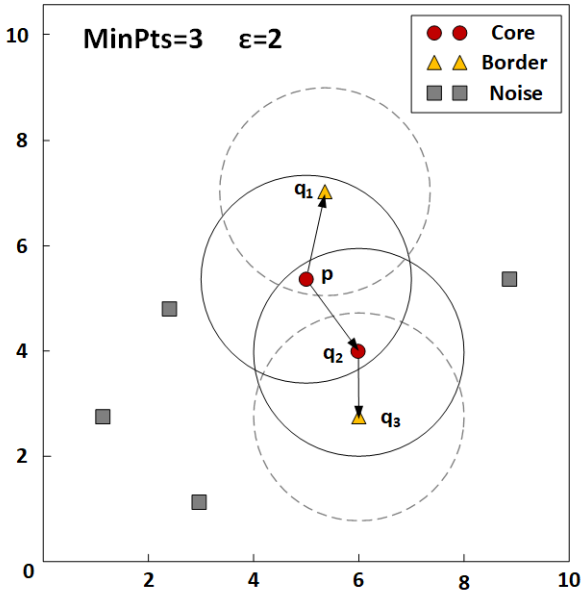

Figure 3.4: DBSCAN algorithm for MinPts=3 and ϵ=2. Point p is a core, since there is a total of 3 points within its ϵ-neighborhood (q_1, q_2, and p itself). Point q_1 is directly density-reachable from p but does not satisfy the core condition and, therefore, is considered to be a border point. Points that do not fulfil these criteria are considered to be noise.

3.7.2 Drug-carrier adhesion

Drug particles can adhere to the surface of carriers in the form of either a mono- or a multi-layered structure. However, not all carriers in contact with drug particles become coated. Particularly at the beginning of mixing, carriers merely touch or compress intact (or partly broken) agglomerates, and no coverage occurs. Accordingly, it is essential to distinguish actual coated carriers from the mentioned exemptions. Drug particles with centers within the $R_c+(2i-1)R_f$ radius of a carrier center were considered to be attached particles in the i^{th} layer (Fig. 3.5). Carriers with fewer than four layers of fine particles were considered to be coated.

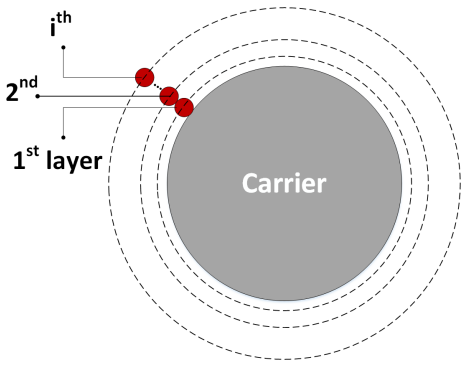

Figure 3.5: Schematic of distance criterion to detect layers of small particles on a carrier.

3.7.3 Adhesive mixing index

Once the number of drug particles adhered to a carrier surface is known, it is possible to calculate the standard deviation of drug particle distribution (σ) using the following

equation:

$$\sigma = \sqrt{\frac{\sum_{i=1}^{N_c}(n_i - \bar{n})^2}{N_c - 1}} \tag{3.2}$$

where N_c is the total number of carriers, and $\bar{n}$ is the equal share of total drug particles for each carrier. The ideal state in adhesive mixing is when all small particles are uniformly and evenly dispersed onto the surface of all carriers, and the standard deviation equates to zero (σ_R). In contrast, the components are fully segregated, and the standard deviation has its highest value (σ_0) at the beginning of mixing. Therefore, the time-dependent index of mixing can be defined as [99]:

$$M = \frac{\sigma_0^2 - \sigma^2}{\sigma_0^2 - \sigma_R^2} = 1 - \left(\frac{\sigma}{\sigma_0}\right)^2 \tag{3.3}$$

The index will have a zero value for a completely segregated mixture and will increase to unity for an ideal ordered mixture. This idea was adapted from the Lacey mixing index [74], which simply denotes the ratio of how much mixing has occurred to how much mixing could occur.

3.7.4 Surface area coverage

Another applicable method used to determine mixture quality in adhesive particle mixing is the surface area coverage (SAC) of carriers. This parameter is defined as the ratio of the total projected area of the drug particles to the surface area of the carrier particles to which the drug particles are attached [17, 16]. According to this definition, the covered area should be calculated based on the number of attached drug particles in the first layer ($n_i^{1^{st}}$). Therefore, an average value of SAC in the system can be expressed as:

$$SAC = \frac{\sum_{i=1}^{N_c} n_i^{1^{st}} \pi R_f^2}{N_c 4\pi R_c^2} \times 100\% \tag{3.4}$$

3.7.5 Particle area and volume

In the context of non-spherical particles, an accurate calculation of the volume and surface area of an entire shape, or a segment of the shape, is often required. This shape rendering was carried out in MATLAB by first reading the corresponding .stl file and then applying the `stlVolume.m` function [72] developed for this purpose.

4

Results

This chapter summarizes the major findings of the present research. These findings include a general method for assessing the quality of adhesive mixing along with the effect of two principal variables, namely particle surface energies and mixing intensity, on the degree of mixing. The results of ternary adhesive mixing simulations are presented in an attempt to shed light on the role of fine excipient particles in DPI-formulation. Lastly, the importance of shape and roughness in the context of adhesive mixing simulations and the dispersion of DPI formulations is addressed.

4.1 Adhesive mixing in a shearing cell (Paper I)

Figure 4.1 shows the initial and final configuration of particles for the blending of 10 drug agglomerates and 200 carrier particles. The temporal and spatial scale of DEM simulations in the figure provides detailed information in order to follow the evolution of mixing. This evolution was investigated from two perspectives including the breakage of agglomerates and the formation of adhesive units.

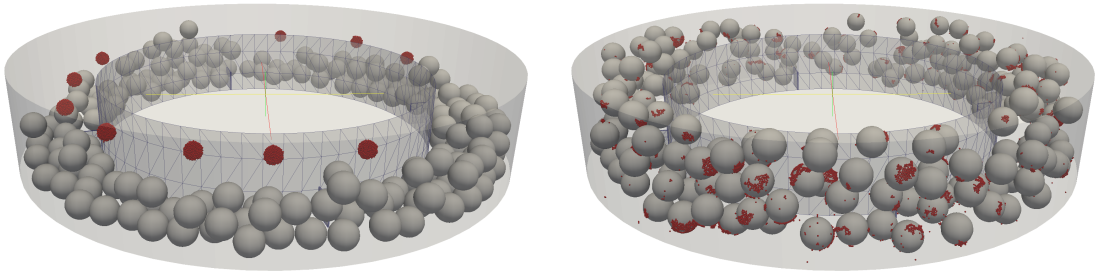

Figure 4.1: (Left) Initial loading of particles; (Right) Particle snapshot after blending for 3.5 sec at 400 rpm.

4.1.1 Agglomerate breakage and fragment sizes

The extent of breakage of the agglomerates is expressed in terms of damage ratio, i.e. the ratio of broken contacts to the initial number of bonds in the agglomerate (D_r) [117]. While the energy imparted to the agglomerate is the cause of damage, the extent of damage at each energy level is determined by the mechanical characteristics of the agglomerate, i.e. if the agglomerate is hard and compact or weak and loose.
A typical behavior of D_r over time in the shearing cell is shown in Figure 4.2. At the beginning of mixing, some new and temporary contacts were formed inside the agglomerates as carriers started squeezing loosely packed agglomerates. A natural consequence of

this compression was a decreasing trend in D_r, resulting in negative values for the damage ratio. However, this decrease lasted for a very short period, and it started increasing as the particles were mixed and agglomerates were completely disintegrated. D_r maintained an increasing trend as the mixing proceeded until it became positive and reached a pseudo-steady value (Paper I).

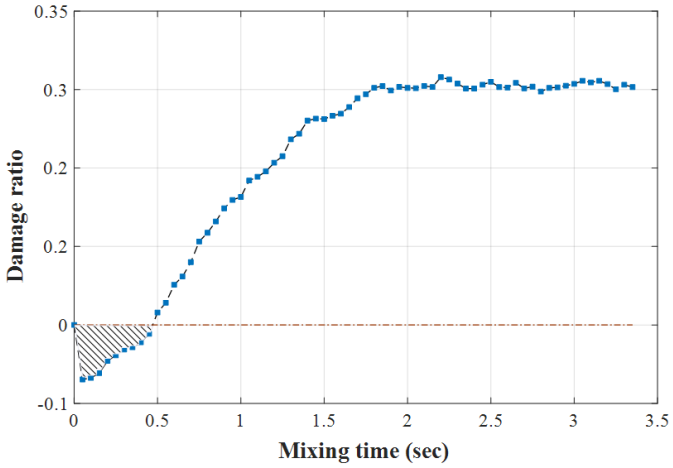

Figure 4.2: Damage ratio versus mixing time. The shaded area corresponds to the time interval when the agglomerate compression is the dominant phenomenon in the mixing.

The DBSCAN algorithm was used to detect and measure clusters of drug particles at each stage of the mixing process. The results of this algorithm are shown in Figure 4.3 as a distribution plot of cluster size. Initially, all drug particles were present in the form of large agglomerates, each containing 1000 primary particles. During the shearing, large agglomerates began to break and generate dozens of fragments. A spatial analysis of clusters revealed that when small sub-agglomerates were produced, they remained in the system for a relatively long time during the mixing (Paper I).

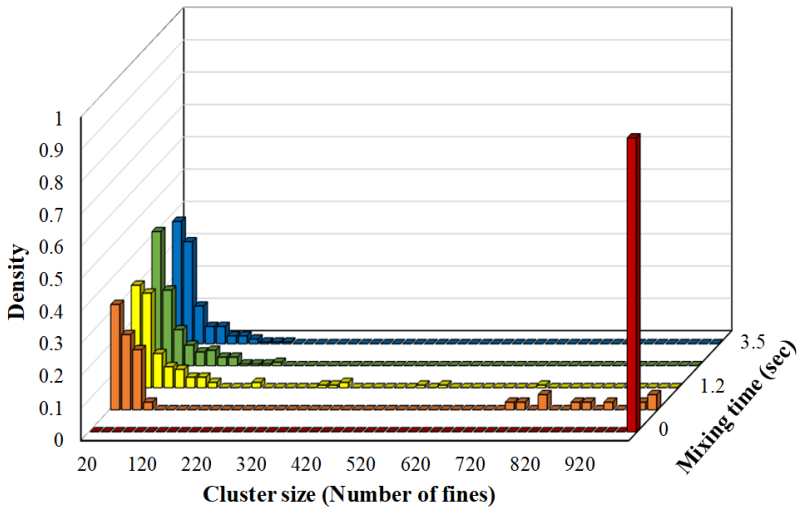

Figure 4.3: Size distribution plot of clusters at different mixing times. Size is represented by the number of constituent drug particles.

4.1.2 Formation of adhesive units

In order to identify the adhesive units in the mixture, information on the established contact between drug and carrier particles were acquired. This number corresponds to the number of captured drug particles, and its evolution over time is shown in Figure 4.4. The formation and development of the coating layers on carriers as well as the drug exchange between carriers can be seen with these bar plots, equivalent to the essential steps that govern the adhesive mixing process (see section 1.1). The area under these bar plots represents the total number of attached drug particles, consequently, it is possible to extract information about the free, unattached drug particles (debris) in the system (Paper I).

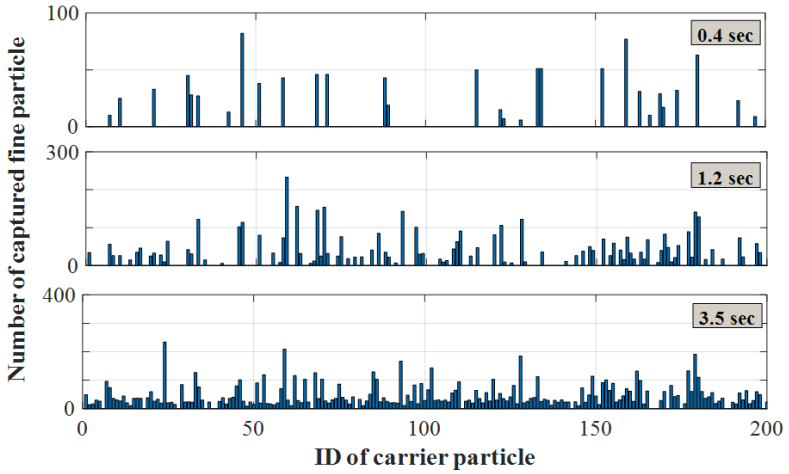

Figure 4.4: Bar plot of the number of attached drug particles on each carrier at different mixing times.

The capture ratio was also used to calculate the mixing index, according to Eq. (3.2) and Eq. (3.3). In addition to the mixing index the number of drug particles on the first layer were extracted and the SAC was computed with Eq. (3.4). The progress of adhesive mixing was ultimately inferred by studying the temporal evolution of these two indices, the agglomerates' D_r, and their deviation from ideal values (Papers I and II).

4.2 Interplay of interaction energies and mixing intensity (Paper II)

The CAB ratio was identified to be a critical attribute in the adhesive mixing process, along with the extent of energy that was provided for blending (see section 2.2). This critical dependency was studied by simulating systems of various particle surface energies that undergo different shearing rates. A variation of surface energies was introduced to drug-carrier (adhesion strength or Γ_{f-c}) and drug-drug (cohesion strength or Γ_{f-f}) interactions according to Table 4.1. Each case was simulated at three impeller speeds of 200, 400, and 800 rpm. Hereinafter, the cases are referred to by their roman number followed by their impeller speed (e.g. I-200).

Table 4.1: Notation of the simulated cases to study the interaction energy of particles and their corresponding values.

		$\Gamma_{f-f}(J/m^2)$		
		0.005	0.01	0.02
$\Gamma_{f-c}(J/m^2)$	0.005	-	Case I	Case II
	0.01	Case III	-	Case IV
	0.02	Case V	Case VI	-

4.2.1 Unifying the parameters

In order to properly link the behavior of an adhesive mixing system to its corresponding values of Γ for particles and mixing energy, these parameters were lumped together in the form of mechanistically motivated dimensionless groups, defined in the next section.

4.2.1.1 Estimation of the Stokes number from energy balance

In a general framework for binder granulation, a critical Stokes (St) number must be reached for the deformation and/or breakage of granules to commence. This number relates the initial kinetic energy in the shearing mass to the internal energy resisting deformation.
Analogous to this number, the St number was defined in adhesive mixing as the entire kinetic energy imparted to the agglomerate over its initial internal resisting energy. The direct integration of the kinetic energy of the rotating wall was used to calculate the energy transferred to the particle in the shearing cell. The internal resisting energy of agglomerates was estimated from the total work required to entirely break up a single contact in the agglomerate (Paper II). Following the JKR theory of adhesive contact, the adhesion work of a single contact is [100]:

$$W_{contact} = \left(\frac{\Gamma_{f-f}^{5} R^{*^4}}{E^{*^2}} \right)^{1/3} \tag{4.1}$$

This work of adhesion was then multiplied by the initial number of contacts in the system (N) to get the total resisting energy of agglomerates. Subsequently, the St number was formulated as:

$$St = \frac{\text{Cumulative kinetic energy}}{N \times W_{contact}} \tag{4.2}$$

4.2.1.2 Estimation of reduced intermixing coefficient

In the context of granulation, a reduced spreading coefficient has been defined as the ratio of adhesive interaction to cohesive interaction strength. Analogous to this coefficient, a dimensionless parameter denoted as the reduced intermixing coefficient (Λ_{f-c}), has been derived for carrier-based DPI formulation by Begat et al. [11]. The value of this parameter with respect to unity is a direct indication of the alacrity ($\Lambda_{f-c}>1$) or reluctance ($\Lambda_{f-c}<1$) of the drug particles to interact with carrier particles.
A similar concept, however with an inverse definition, was used in the present work for the analysis of adhesive mixtures based on the values of Γ_{f-f} and Γ_{f-c}. This non-dimensional coefficient is expressed as:

$$\Lambda = \frac{\text{Cohesion strength}}{\text{Adhesion strength}} = \frac{\Gamma_{f-f}}{\Gamma_{f-c}} \tag{4.3}$$

4.2.2 A regime map for quality of adhesive mixing

The conducted simulations revealed that it was of vital importance in an adhesive mixing system to maintain a balance between the St number and the Λ coefficient, otherwise the blending process resulted in a mixture with poor quality. The intention was to identify and classify conditions that lead to such unwanted mixtures.
At the pseudo-steady state of mixing, simulated cases are divided into three classes corresponding to low, medium, and high ranges of the St number. These cases are equivalent to systems with: (i) insufficient, (ii) sufficient, and (iii) excess input energy levels, respectively. Evidently, the limits to distinguishing these energy levels and the dynamic features of adhesive mixing are intertwined with the system's Λ coefficient. The simulated cases were, thereby, divided into the following groups, representing both desired and undesired adhesive mixture (Paper II):

- **Sufficient input energy**
  The process started with the compaction of the loose initial agglomerates by collisions with adjacent carriers. This led to the generation of new particle contacts that translated as a negative damage ratio. Soon after this, agglomerate disintegration started, and the D_r increased steadily. The disintegration of agglomerates generated an individual or a cluster of drug particles that adhered to the surface of the carriers, thus gradually increasing the SAC and mixing index.

- **Excess input energy: Detachment of drugs from carriers**
  Cases in which the imparted energy was excessive were characterized by an intense breakage of agglomerates. This breakage provided a large number of free drug particles that could adhere to carrier surfaces. However, the high rate of collision

among carriers detached the deposited drugs from the host carriers and created an abundance of debris. The temporal evolution of the mixing index and the SAC signified that, initially, the coating progressed with time, however, the mixing index and SAC both levelled out at comparatively low values, indicating poor mixing.

- **Insufficient input energy**
  If the energy imparted to particle assembly was too low, the system behaved in two different ways depending on the Λ coefficient:
  - **For $\Lambda > 1.0$: Coalescence of agglomerates**
    The agglomerates remained almost intact under shearing. A further increase in Λ resulted in a tendency for the agglomerates to coalesce and form larger agglomerates. Not only were the agglomerates unbroken, but the 10 initial aggregates had merged into four larger ones. Therefore, the D_r dropped to negative values and decreased steadily. Consequently, no coating happened and the mixing index and SAC remained zero over time.
  - **For $\Lambda < 1.0$: Lumping of carriers**
    The agglomerates broke easily, however, the mixing quality was poor due to the jamming of carrier particles in the system. The variation of the D_r showed the successive occurrence of agglomerate compression ($D_r<0$) and breakage ($D_r>0$). The weak cohesion between primary particles in the agglomerates promoted their disintegration even under the lowest shear rates. However, the progressive distribution of drug particles over carriers ceased as a result of the carrier tendency to jam. Therefore, the mixing index and SAC did not develop well, indicating poor mixing.

It must be pointed out that the extent of variation in these parameters was intended to understand the extreme behaviors of the system and to fathom the dominant mechanism at each condition. This fact, however, does not imply that these conditions rarely occur in reality (experimental data in Paper II).
The results were utilized to construct a semi-quantitative regime map for the quality of adhesive mixtures as a function of the two most prominent system variables (Fig. 4.5), an idea that originated from the well-known growth regime map for liquid-bound granules by Iveson et al. [64]. This descriptive map assigns all simulated cases to desired and undesired regions as a function of St and Λ, wherein each region is named after its corresponding dominant phenomenon in the shearing cell. Although the proposed regime map is solely based on two variables and is considered to be a preliminary tool, the idea of foreseeing mixture quality was tested by using the available experiments akin to the performed simulations. For this purpose a series of experimental data on the DPI formulation process were collected from AstraZeneca Pharmaceutical R&D. Certain limitations of this map are also discussed in detail in Paper II.

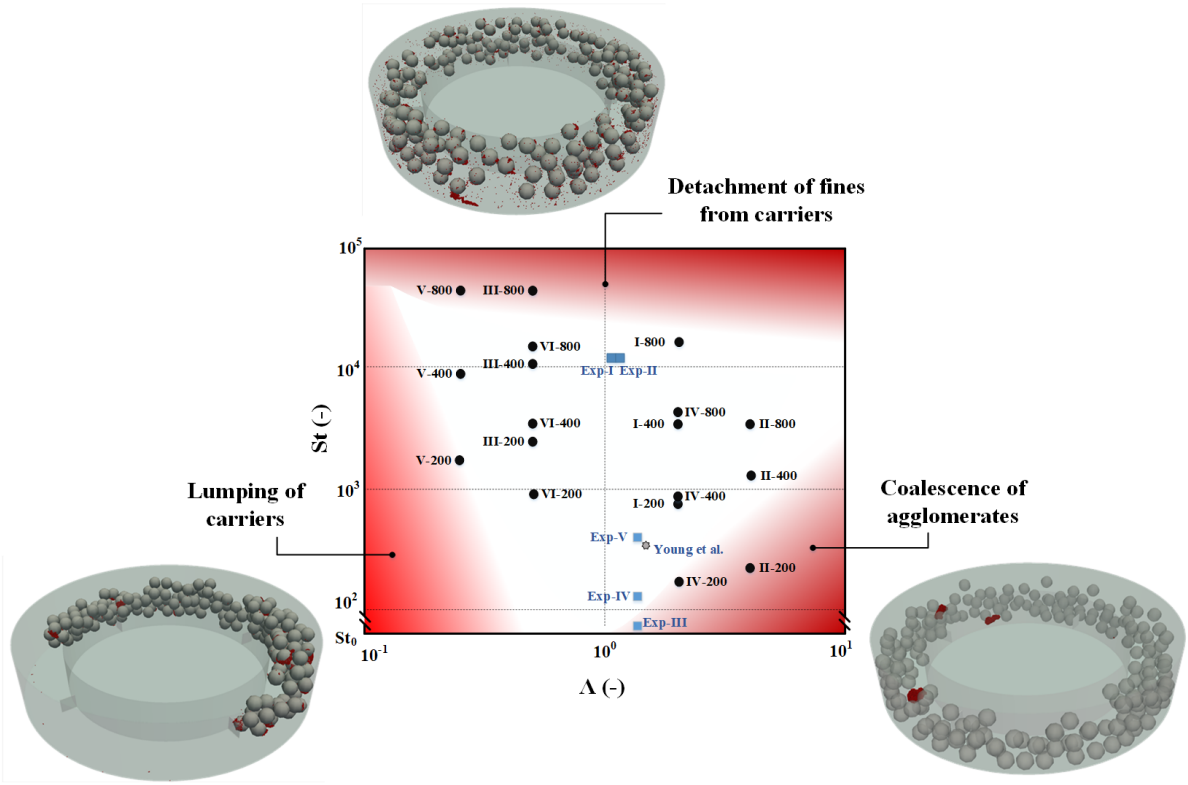

Figure 4.5: Regime map for the quality of the adhesive mixing process based on the interaction energy of particles and mixing intensity.

4.3 Impact test with non-spherical carriers (Paper III)

The geometric attributes of carrier particles, including surface roughness and shape, pose a formidable challenge to the performance of DPI formulation. First, the dispersion rate of fine particles depends on the effective pull-off force between carrier and drug particles. This force is affected by the irregularity and/or roughness of the carrier surface. Second, the variation in carrier shape and morphology have a natural impact on the formulation process since these features can change the breakage pattern of agglomerates and the extent of drug particle deposition over carriers during blend preparation (Paper III).
In order to understand the importance of these factors in a fine temporal and spatial resolution, a DEM simulation of an impact test was conducted on a series of carrier particles with predetermined shape and texture. The simulations helped to control the collision parameters more carefully. Complex-shaped carriers were mathematically described using the Fourier harmonics (see section 2.4.6.1). Despite the natural dependency of shape, roughness, and surface energy of each carrier particle on those of other carrier particles, this technique provided the possibility to confine the study to the effect of carrier shape and texture.

4.3.1 Selection of complex-shaped carrier particles

While each Fourier descriptor represents an intrinsic feature of particle shape, it has been found that three descriptors, known as signature Fourier descriptors, convey considerable information on particle shape [110]. The D_2 controls the elongation of particles, the D_3 is responsible for the main irregularities of the overall particle shape, and the D_8 provides information on the asperities of a particle.
A factorial design was therefore used to create carrier particles with different morphologies. Two levels were assigned to each signature descriptor, resulting in 8 cases. The low level was zero for all descriptors and the high level was 0.1 for D_2, 0.05 for D_3, and 0.015 for D_8. These values were selected in a way that resembled elongated, irregular, or rough particles (Paper III). The detailed information on simulation parameters as well as the corresponding shape factors for each carrier can be found in Paper III.

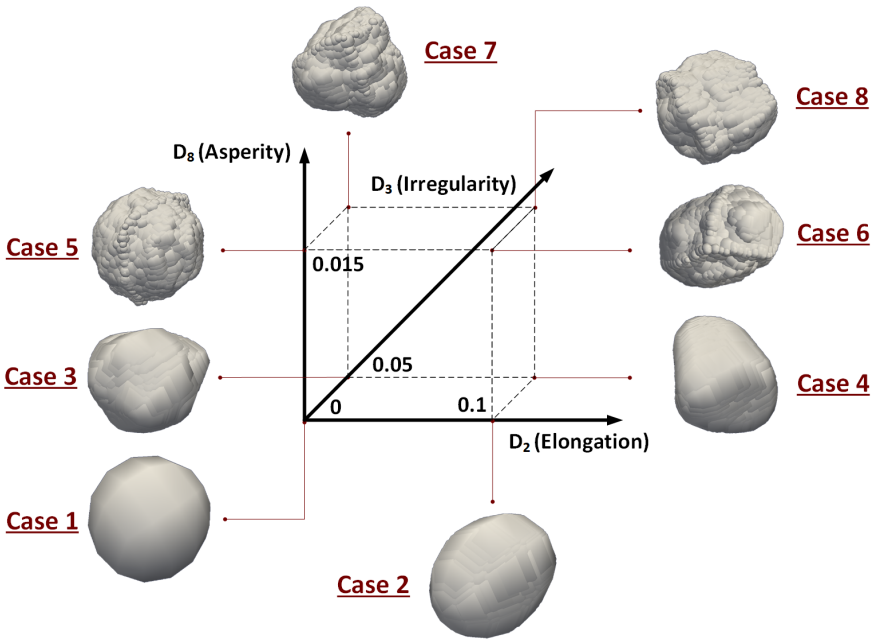

Figure 4.6: Representation of the complex-shaped particles generated for this study. Three axes denote the signature Fourier descriptors and their corresponding effect on the shape and morphology of a particle.

4.3.2 Analyses of the impact

4.3.2.1 Damage ratio

The impact test was carried out at two different collision velocities of 4 and 6 m/s, corresponding to the Δ number of 30 and 68. These values were selected to ensure that the kinetic energy would suffice for agglomerate break up [94]. The low surface energy of drug particle implies that the agglomerate breaks in the ductile mode, a failure mode dominated by extensive deformation followed by disintegration into small fragments. This was observed by an initial compression of the agglomerate (D_r<0) and further breakage of internal contacts between primary particles (D_r>0) (Paper III). The collision pattern was analyzed at the completion of the agglomerate-target impact. Apart from D_r, the capture ratio, as a metric to quantify the deposition of drugs over different carriers and the

largest fragment size as a metric to study the effect of carrier shape on the agglomerate disintegration was selected to explore the behavior of agglomerate upon impact.

4.3.2.2 Capture ratio

Figure 4.7provides an overview of some of the simulated cases. The capture ratio exhibited a strong dependency on carrier shape insofar as it had values close to the lowest and highest limits of the ratio (Paper III). For each carrier particle, the impact test was carried out at eight different directions, of which three were orthogonal. The simulation results also revealed that the deposition of drug particles on one individual carrier target strongly depend on the collision direction.

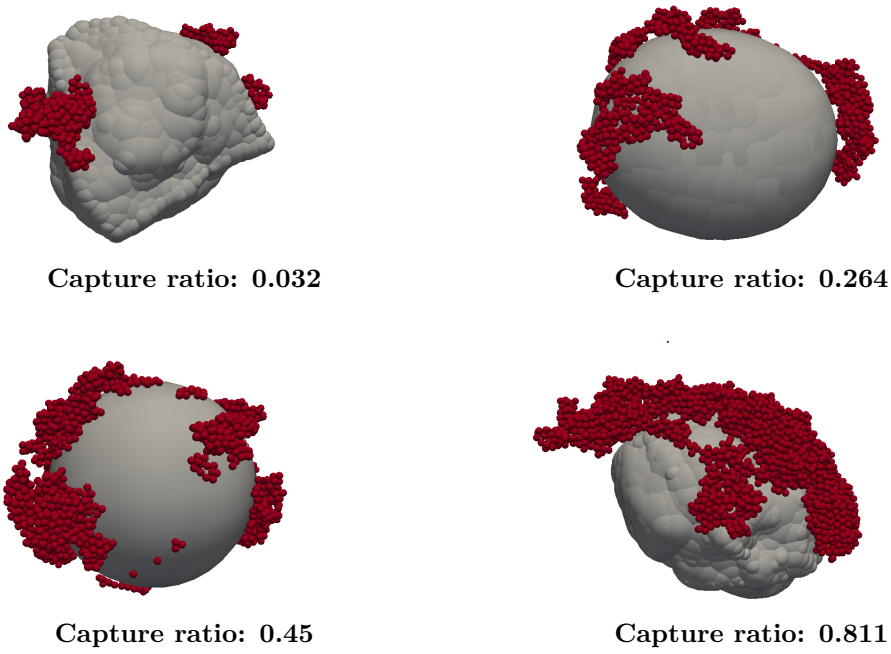

Capture ratio: 0.032 **Capture ratio: 0.264**

Capture ratio: 0.45 **Capture ratio: 0.811**

Figure 4.7: Overview of drug particle deposition on different carrier particles and their corresponding capture ratio.

The extent of this dependency was further quantified by conducting an ANOVA test on the results (Table 4.2). The calculated sum of squares (SS), the degrees of freedom (DF), and the mean value of SS (MS) for each source of variation are reported in the table. The statistical F-value was then calculated based on the estimation of variances, and the significance of each term was investigated. The ANOVA test, with a 99% significance level, showed that the D_8, or particle roughness attribute, has a considerable effect on the capture ratio of drug particles (Paper III).

Table 4.2: ANOVA table for the effect of signature Fourier descriptors on capture ratio, with 8 repetitions. Considering a significance level of 99%, the D_8 is an important source of variation in the capture ratio.

Source	Adj. SS	DF	Adj. MS	F	Prob.>F
D_2	0.0178	1	0.0178	0.69	0.410
D_3	0.0443	1	0.0443	1.71	0.196
D_8	0.3255	1	0.3255	12.55	0.001
Error	1.5565	60	0.032	-	-
Total	1.9443	63			

The extent of drug particle deposition, and its standard deviation, showed a striking dependency on the global shape factors of the target particles (Paper III, Figure 7). The capture ratio was lower on average for particles with low roundness. It was also noted that the variation within each case is related to particle sphericity. The results showed that sphericity can be regarded as an indication of particle symmetry, where the capture ratio is less dependent on the direction for a symmetrical particle (i.e. smaller standard deviation for capture ratio), and vice versa.

An interesting observation was that the peak size in the collision zone, and not the overall particle shape, provoked major differences in breakage pattern. It was supported by the fact that, a similar capture ratio was obtained for different collision scenarios. It was, therefore, recommended that, rather than an overall shape factor for a carrier particle, an index should be introduced to measure the size of local peaks in the collision zone. Formulating such an index is particularly challenging for surfaces with asymmetric peaks of different sizes in 3D space.
In this study, a simple and efficient measure was proposed to quantify the size of the local peaks in the collision zone, which is defined as the volume of the carrier segment engaged in the collision, up to the maximum compression of the agglomerate. This governed volume was normalized using the corresponding value of case 1 to indicate deviation from a spherical carrier and was denoted as normalized peak size (see Fig. 4.8). The normalized peak size is less than unity if the collision zone is flat, and it is greater than unity if the collision zone has local asperities and irregularities. The correlation between normalized peak size and drug particle adhesion was investigated (Paper III, Figure 9). The capture ratio was high when the impact happened over the flat side of a carrier, and in contrast, the capture ratio was low when the agglomerate collided with a surface peak.

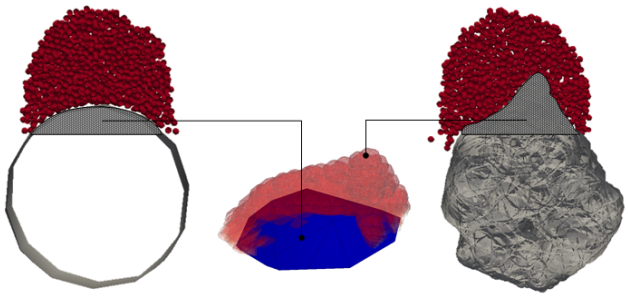

Figure 4.8: The schematic procedure of calculating normalized peak size. Once the agglomerate is fully compressed, the segment of the carrier that is engaged in the collision is extracted and its volume is calculated.

4.3.2.3 Agglomerate fragmentation

A different perspective on collision is obtained by examining agglomerate fragmentation. The size of generated fragments after impact, mostly the 1^{st} and 2^{nd} largest, have been extensively studied in the context of detecting breakage regimes for spherical agglomerates [49]. In the present study, the size of the largest surviving fragment after collision was extracted for each carrier. The values of largest fragment size were then normalized according to the size of the initial agglomerate ($N_{Fragment}/N_0$) and are plotted in Figure 4.9. By comparing the shape factors of target particles with values in Figure 4.9, it is evident that the elongation factor contributes to the generation of large fragments. This factor also affected the variations in the largest fragment size for each case, depending on the collision direction (note the width of error bars for Cases 2, 4, and 6).
An analysis of variance was used to correlate between signature Fourier descriptors and the largest fragment size (Paper III, Table 4). The elongation and irregularity characteristics of the carrier particle were found to have a significant effect on the size of the largest fragment after impact. A relative comparison between spherical and elongated target particles showed that the spherical carrier generated more fragments than the elongated one (10 vs. 3), nevertheless, the spherical carrier had comparatively smaller fragment sizes (Paper III, Figure 11).

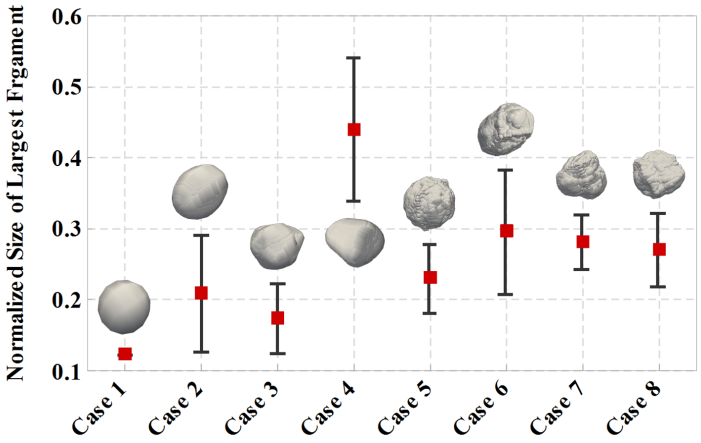

Figure 4.9: Normalized size of the largest surviving fragment. The elongation factor affects the size of the largest fragment.

4.3.2.4 Distribution of capture ratio and largest fragment size

The dependency of capture ratio and the size of the largest fragment on collision direction suggests that reporting an average value for each carrier can be misleading. Instead, it is more informative to study the behavior of these indices by looking into their probability distribution. To do so, a more elaborate impact test was conducted by assigning 30 different collision directions. These directions were selected by generating random points around the carrier particle at a specific radius and using them as the starting point of the agglomerate motion.
The distributions of these parameters were plotted after post-processing the resultant impacts and calculating the capture ratio and the normalized size of the largest fragment (Figure 4.10). By fitting a probability function to these distributions, such plots can be beneficial in simulating adhesive mixture systems containing a large number of irregular carriers since they can bridge information from the microscopic to the macroscopic level

and save computation time (e.g. implementation in population balance modelling).

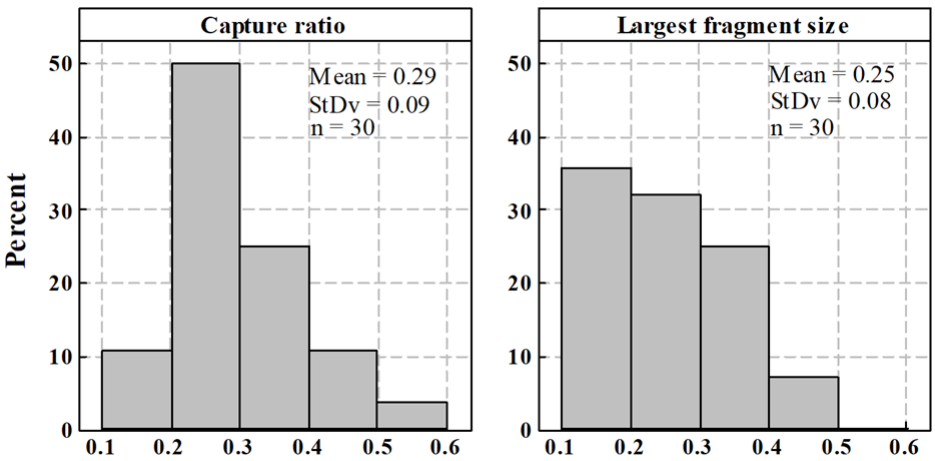

Figure 4.10: The distribution plot of capture ratio and the normalized size of the largest fragment after impact for an elongated carrier (Case 2).

4.4 Adhesive mixing in vibrating cell (Paper V)

Once the significance of carrier particle shape in the context of a single agglomerate breakage had been addressed, attention was devoted to resolving a more complicated feature of adhesive mixing systems. This feature, which also demands using a complex-shaped carrier particle, concerns the possible advantages of ternary over binary DPI formulation. See section 2.6 for a brief discussion of the inclusion of fine excipient particles as a third mixing component in the binary blend of drug and carrier particles.
A number of binary and ternary adhesive mixing systems were, consequently, simulated in a simple vibrating cell in order to shed light on the role of fine excipient particles in adhesive mixing.

4.4.1 Creating a coarse particle for ternary system

An integral feature of DEM with a multisphere model is that it supports the local contact properties of the single particle to be manipulated, including the radius of curvature. This feature allows the creation of a particle with a targeted distribution of surface adhesion force, e.g. a log-normal distribution. For this purpose, a series of Fourier shape descriptors were obtained from real particle shapes, and the corresponding coarse carrier particles were generated in the simulation domain. Once the carrier particle had been generated, the adhesion force distribution was extracted based on the following steps:

1. A stable adhesive unit was created by randomly placing 2000 adhesive micronized particles over the carrier particle.

2. The magnitude of the adhesion force between the carrier and small particles was obtained and turned into a dimensionless quantity by using the corresponding minimum and maximum values. In this way, the non-dimensional adhesion force distribution becomes a unique feature of a coarse carrier particle.

The distribution of the dimensionless adhesion force was examined, and the carrier with the closest fit to the log-normal distribution (analogous to the experimental data presented in Figure 2.8) was selected for the purpose of this study. Figure 4.11 shows the selected carrier with 2000 adhesive particles of 2 μm diameter deposited over its surface as well as the corresponding distribution of the non-dimensional adhesion force. The selection of this carrier particle, despite the slight deviation in the log-normal fit, is elaborated in Paper V.

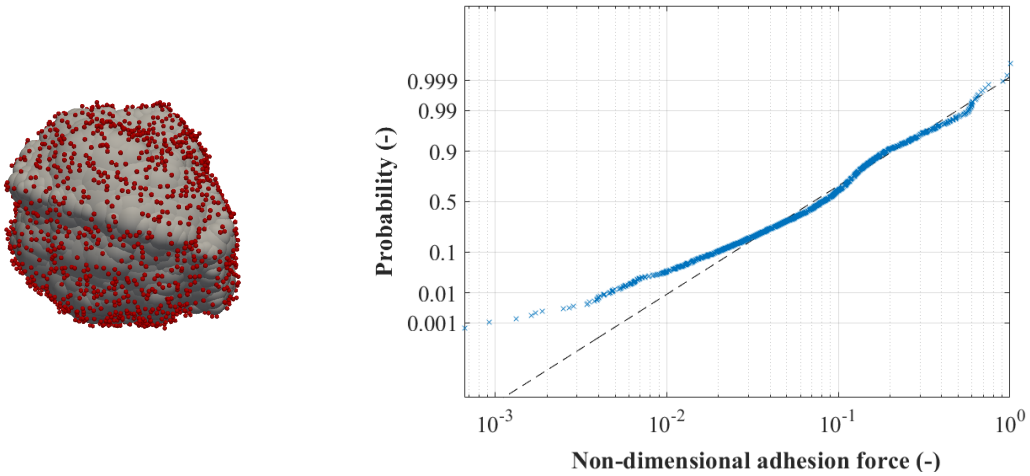

Figure 4.11: (Left) The adhesive unit selected to study the ternary system; (Right) Distribution of the non-dimensional adhesion force of the selected carrier.

4.4.2 Case studies

The simulations were planned and conducted according to Table 4.3. They comprise one binary and two ternary formulations with different levels of fine content. See Paper V for a thorough explanation of the validity of these parameters compared to the experimental range of data, and the additional steps in the simulation setup, including the order and form of particles that were inserted into the mixing cell.

Table 4.3: Case studies for investigating the differences between binary and ternary adhesive mixing. * The loading ratios are expressed compared to carrier particles.

Case No.	$d_{Drug}(\mu m)$	Drug ratio* (%)	$d_{Fine}(\mu m)$	Fine ratio* (%)
Case I	3	1.32	-	-
Case II	3	1.32	5	5.7
Case III	3	1.32	5	12.2

4.4.3 From binary to ternary: Mechanistic effects of fines

To unravel the role of fine excipient particles, the evolution of mixing was scrutinized by examining the breakage of agglomerates of fines and drugs, the deposition of particles over coarse carriers, the strength of adhesive forces, and the structure of attached layers. Case I and Case II were analyzed to pinpoint these mechanistic differences.

4.4.3.1 Breakage of agglomerates

The rate of drug agglomerate breakage was examined by studying the temporal decay in the average coordination number of these particles. The coordination number was extracted at each time step and was normalized by dividing it by its maximum value, which was obtained from the initial agglomerate condition. Figure 4.12 displays the normalized drug coordination number for both binary and ternary mixtures over time and marks the disparity in agglomerate breakage for these two systems. Even though both systems were mixed under similar conditions, the inclusion of fine excipient particles hindered agglomerate breakage.

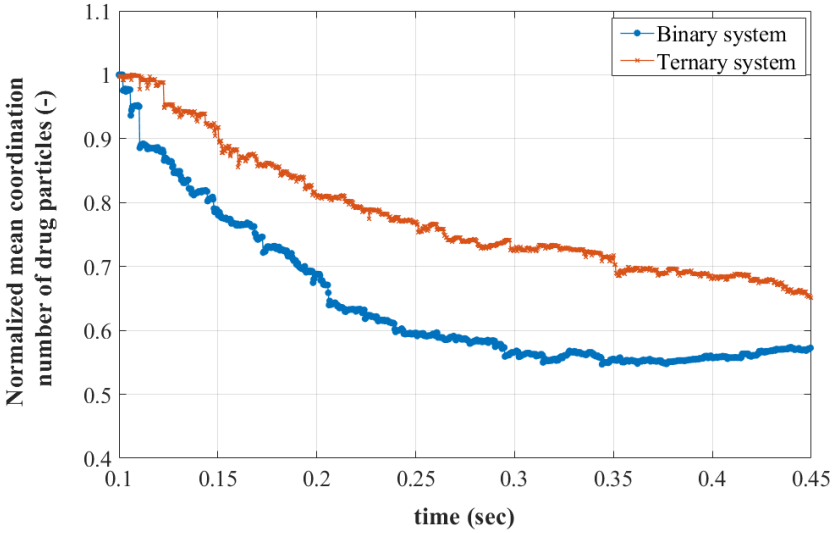

Figure 4.12: Temporal decay in the average coordinate number of drug particles for ternary and binary systems.

Besides the rate of drug agglomerate breakage, it was of interest to study the evolution of clusters of fine excipient particles during mixing. Although the primary fine particles were introduced individually into the system, they started to form clusters as contact was established. This phenomenon can be observed by examining the temporal progress of fine-fine contacts at early stages of the mixing (Paper V, Figure 7(a)). The number of inter-particle contacts of fines increased sharply after the vibration started, and it decreased as the mixing progressed, due to the breakage of clusters. Compared to the drug agglomerates, these clusters were weaker, more irregular in shape, and had a broader size distribution (Paper V, Figure 7(b)).

4.4.3.2 Structural analysis of adhesive units

A comparatively lower breakage rate for drug agglomerates in a ternary system did not necessarily indicate a poorer degree of mixing for such systems. An assessment of drug particle distribution over the carriers revealed that, in the final state of mixing, all the drug particles had adhered onto the carrier surface, although in different forms. This difference was attributed to the contrast between forming a monolayer or a multilayer distribution of drugs over carriers.
Figure 4.13 shows the number of carrier-drug direct contacts for the binary and ternary systems. Normalization was done after dividing each value by the total number of drug

particles. Once the mixing of the binary mixture was completed, 97% of all drug particles had been spread over the carrier particles. For the ternary system, a lower percentage of drugs (85%) had directly adhered onto the carriers. This disparity signifies that, contrary to the binary system, the drug particles in the ternary system are more likely to attach to carriers in the form of small aggregates. This observation suggests a possible advantage of ternary formulation in aerosolization performance, similar to the assumptions behind the agglomeration theory.

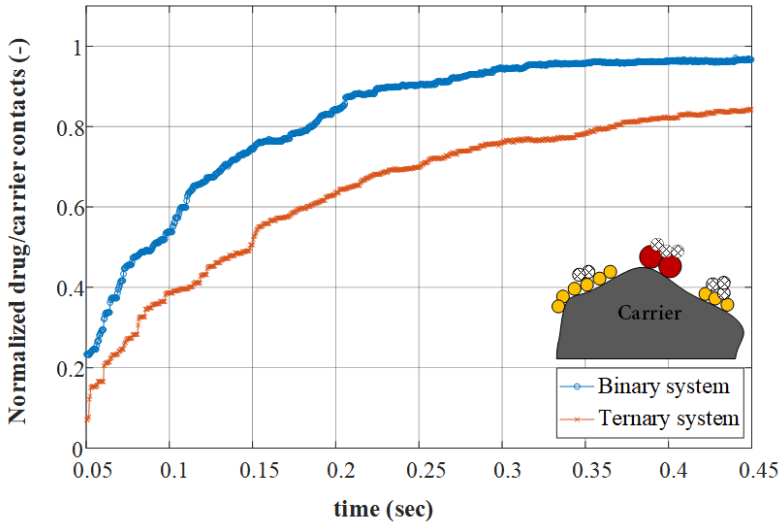

Figure 4.13: Temporal deposition of drug particles over carrier particles for binary and ternary systems. Only direct contact with the carriers are counted (red: fines, yellow: drug with direct contact, white: drug with indirect contact).

DEM results showed that, in the course of mixing, the average kinetic energy of carrier particles was alike for both systems, however, the rate of particle-particle and particle-wall collisions for carriers was significantly lower in the presence of fine particles (Paper V, Figure 9). Analogous to what the buffer theory suggests, it was observed that the fines reduced carrier particle collisions and, thus, protected drug particles from impact.

4.4.3.3 Assessment of active site theory

Once the mixing was completed, the adhesive contact between carrier-drug and carrier-fine was determined in order to identify possible differences in attachment patterns. The adhesion properties, including the contact force and local contact position for each particle, of each carrier surface were obtained. A comparative probability distribution of adhesion forces suggests that, if the active site theory is at work, the carrier sites with lower activity will be covered by drug particles (left tail of the distribution), and the highly active sites of the carrier will be occupied by fine particles (right tail of the distribution).
Figure 4.14 shows the distribution of the average adhesive contact force; the carrier-drug and carrier-fine contacts are distinguished by two colors. It can be seen in the figure that these two distributions are closely matched, implying that the suggested competition between drug and fine particles to adhere onto carriers, as proposed by the active site theory, is not evident. This finding is supported by previous experimental observations that contradict the active site theory: the insignificance of blending order on formulation

performance [84], the ability of drug particles to displace the fines from their carrier binding sites [80], and the ambiguous effect of carrier particle size on the FPF reported by Islam et al. [62].

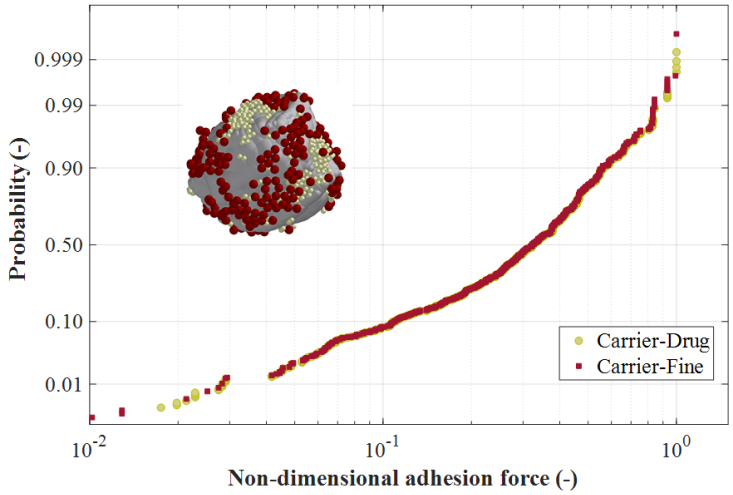

Figure 4.14: Distribution of adhesive force for carrier-drug and carrier-fine contacts at the completion of ternary mixing. The graph suggests that there is no preference for saturation of carrier active sites by either drug or fine particles.

4.4.4 The effect of fine loading ratio

An intricate aspect of ternary DPI formulation is that the dispersion performance relies on the attributes of the added fine particles, including loading ratio and size. While the influence of particles size was briefly discussed in the context of the validity of the buffer theory, the effect of the loading ratio requires further exploration. For this purpose, case III was analyzed and the outcomes were compared to the earlier findings of the present work.
Analogous to the behavior at the transition from binary to ternary formulation, the breakage of drug agglomerates was further suppressed at a higher loading ratio of fine particles. Comparing the size distribution of drug agglomerates in the three systems, as displayed in Paper V, Figure 11, it was found that drug agglomerate breakage slowed down as more fines were introduced into the system, and the surviving agglomerates became larger. This behavior resulted in poor mixing because the drug particles did not distribute equally among carrier particles.

While the addition of 5.7% w/w fine particles into the binary system was found to have a negligible effect on the kinetic energy of carrier particles, increasing the mass fraction of the fine particles to 12.2% imposed a noticeable effect on the total kinetic energy of the carrier particles. Figure 4.15 shows the cumulative kinetic energy of carrier particles for three adhesive mixing systems. The translational and rotational components of the kinetic energy are displayed separately. A major change that ensued from the excess of fine particles was a significant decrease in the rotational kinetic energy of coarse particles. This behavior was attributed to the aggregation of coarse particles due to the cohesion of fine particles and the resultant constraint on the dynamic behavior of the carriers. The slow breakage rate for drug agglomerates in the ternary system of 12.2% w/w fines can also be explained in terms of inefficient energy transition to the drug particles due to the collective

motion of coarse particles and lack of inter-particle collisions. This phenomenon has been discussed by Shur et al. [108] in the context of the aerosolization process, wherein the cohesion of fines was found to increase the tensile strength of the entire powder bed, and therefore, the particles moved as a plug. Those authors have argued that this behavior is in favor of the dispersion process because the cohesion of fines shifts the MFV. However, the authors have not explained how the dispersion enhancement is therapeutically achieved if the expiratory flow rate is obstructed, as is normally the case with patients suffering from chronic respiratory diseases.

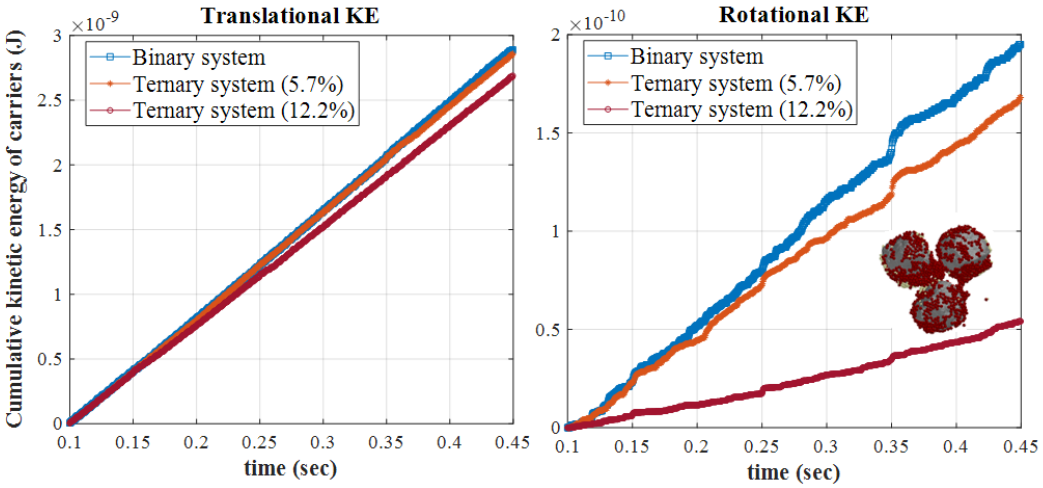

Figure 4.15: Cumulative kinetic energy (KE) of coarse particles in three systems decomposed into translational and rotational components. The particle assembly is lumped together due to the cohesion of fine particles, and their relative rotation decreases significantly.

4.4.5 Evaluation of drug dispersion

In order to evaluate the performance of ternary formulations compared to binary one, the dispersion behavior of each blend was examined according to the following procedure. After the mixing was finalized, the vibrating cell was removed from the simulation domain and the particles assembly, under the influence of gravitational force, were accelerated until they collided with a rigid wall in the normal direction. With this configuration, particle dispersion at five different velocities (corresponding to the average velocity of carrier particles) was tested. The FPF was calculated by obtaining the number of detached drug particles after the collision was completed.
Figure 4.16 shows the variation of drug FPF with impact velocity for three different formulations. While the FPF increases steadily with impact velocity for all cases, the lowest dispersion efficiency corresponds to the binary formulation. This indicates the improved performance of ternary formulations over binary system. However, the highest efficiency is observed for the ternary formulation with 5.7% of fine particles, which corroborate to our findings that excess of fine particles does not improve the drug dispersion.

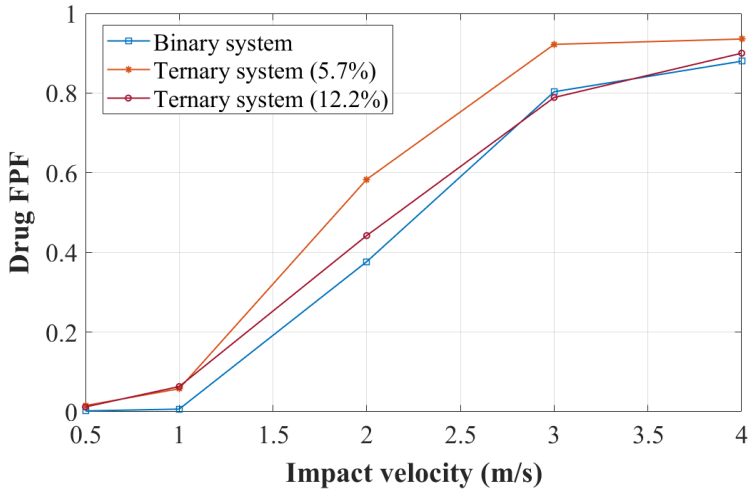

Figure 4.16: Dispersion of drug particles as a result of wall-collision at different impact velocities.

4.5 Role of roughness on dispersion performance (Paper IV)

The role of principal variables in the performance of DPI formulation has been examined thus far, however, the ultimate optimization of drug delivery via inhalation also requires a fundamental understanding of the dispersion process. Consequently, the simulation tools and the methodology that were developed were deployed to understand one key aspect of the drug dispersion process. It is well recognized through several *in vitro* aerosolization tests on carrier-based DPI formulations with carriers of different size, shape, and roughness, that the carrier morphology imposes a profound and yet inconsistent effect on dispersion. A noticeable example of inconsistency in findings pertains to the variation of FPF with carrier surface roughness.

The flow-induced and collision-induced dispersion mechanisms have been captured through extensive multi-scale simulations of the inhalation process by means of combined CFD-DEM modelling. The insightful findings of the latter approach have revealed an extremely high wall collision rate experienced by the carriers and the dominance of particle-wall collision energy over inter-particle collision energy in the dispersion process. Despite the significant role of carrier particle-wall impact in the detachment of APIs, the crucial feature of carrier particle surface roughness has been overlooked in all simulation works so far. Therefore, an elaborate examination of the impact-induced dispersion of APIs was conducted in order to fill the theoretical gap in the modeling context of DPIs and the undetermined behavior of FPF in the presence of surface roughness of carriers. A series of simulations was performed on the dispersion of adhesive units that consisted of carriers with different length scales of roughness.

4.5.1 Generating carrier particles with roughness

Six individual spectra of normalized Fourier descriptors were selected to add controlled roughness to a carrier particle. The choice of Fourier spectrum was based on the following considerations:

- To avoid the differences that the collision of an asymmetrical carrier particle may cause, the overall shape of the particle was maintained nearly spherical. Therefore, the Fourier descriptors that impose elongation or irregularity on a particle shape were kept at zero. The selected elements to be tuned to add roughness were D_{10} to D_{60}.

- Each individual Fourier spectrum adds one independent scale of roughness to a particle surface. In this way, a uniform distribution of roughness summits over the particle surface could be achieved.

- The magnitude of the Fourier descriptor was the same for all cases in order to acheive a similar amplitude of roughness.

The resultant particles with different surface roughness are shown in Figure 4.17. In addition to the rough particles, a smooth spherical particle was included in this work for the sake of comparison.

Figure 4.17: Representation of carrier particles used in this study. These particles are denoted, from left to right, **Carrier 0** to **Carrier VI**.

4.5.2 Analysis of particle surface roughness

The 3D convex hull of a particle was used to extract the surface profile of the particle. In order to capture the variation of surface asperities on different sides of the particle, three orthogonal cross-sections of the particle were chosen to acquire the position of surface points (Fig. 4.18). The polar radius of each point was then compared with a reference distance (the radius of the volumetric equivalent sphere of the particle), and the surface profile was obtained. These surface profiles together with Eq.(2.32) and Eq.(2.33) lead to an average value for surface roughness and rms.
The calculated values of R_a and rms for the carrier particles of this study can be found in Paper IV, Figure 5. Throughout this report, the correlation between collision-induced dispersion performance and the roughness of carriers is expressed in terms of the latter value, since this is a well-recognized index used to describe the surface roughness of inhalable particles.

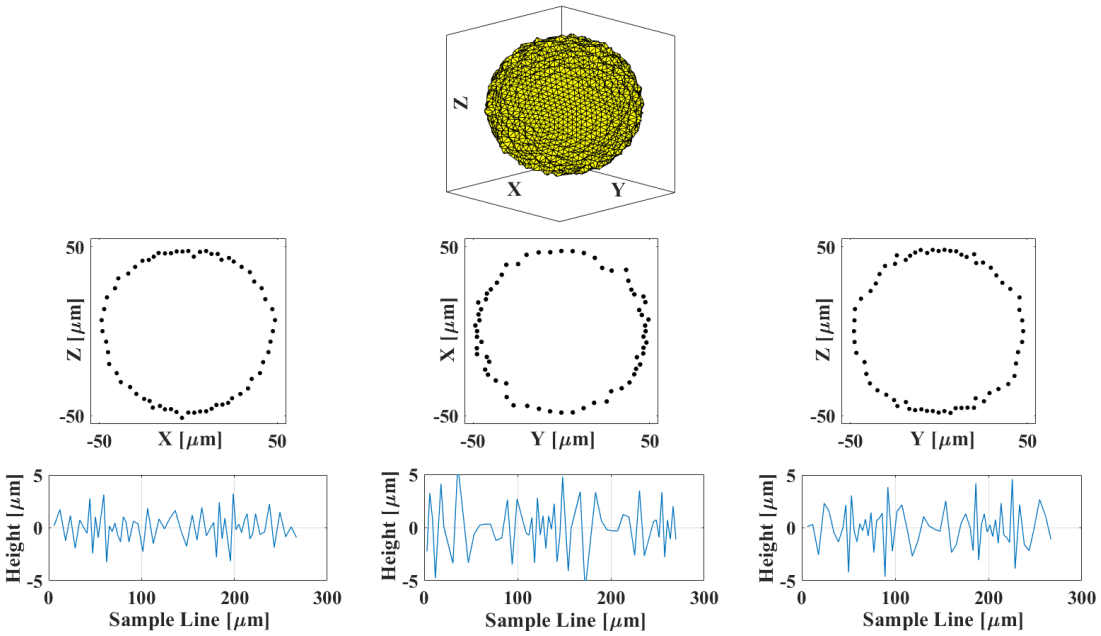

Figure 4.18: Extraction of the surface profile for a complex-shaped carrier.

4.5.3 Evaluation of dispersion ratio

Once an adhesive unit had formed, it was set to collide with a rigid wall in the normal direction at six different impact velocities ranging from 2 to 7 m/s. These impact velocities correspond to the numerical studies on the motion of carrier particles in a typical swirl-flow inhaler device [21]. It has been reported that the probability of flow-induced dispersion at these relative velocities is quite low, and wall collision is the controlling mechanism for the detachment of drug particles.

In order to evaluate the efficiency of drug particle detachment, a dispersion ratio similar to FPF was defined. This was the ratio of the number of drug particles detached from the carrier to the total number of drug particles. Once impact between carrier and wall was completed, the number of detached drug particles was acquired, and the dispersion ratio was calculated. The dispersion ratio was compared with the rms of the carrier roughness of each collision velocity, as illustrated in Figure 4.19 (Paper IV).

It was observed that surface roughness had a direct effect on the dispersion ratio for carrier-wall collision. This behavior is in good agreement with the experimental findings of Tan et al. [112], where a nearly linear relation was discovered between the released FPF and the average roughness of different surface-modified carrier particles. As the outcome of their work shows in Figure 4.20, the positive gradients of all the best-fit lines for different roughness scales and the FPF clearly prove that increased surface roughness contributes positively to dispersion performance.

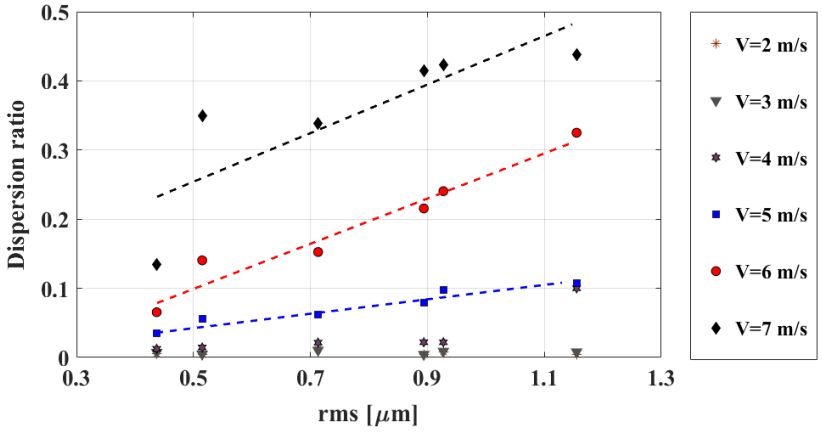

Figure 4.19: Variation of dispersion ratio with the roughness rms of carrier particle surface at different collision velocities.

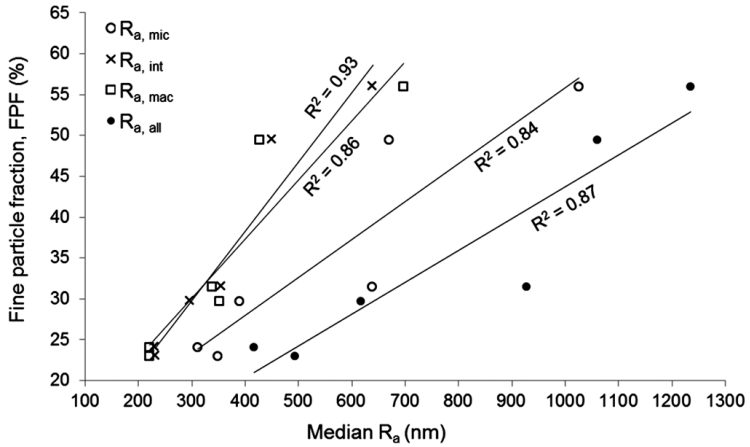

Figure 4.20: Relationship between different scales of roughness parameters for lactose carriers with the fine particle fraction of DPI formulations [112].

The insignificant dispersion ratio of drug particles below a certain impact velocity is shown in Figure 4.19. This finding, alongside the findings of Yang et al. [132, 133], suggests that dispersion performance can be characterized by the balance between impact energy and the total adhesion energy. This energy ratio is formulated as:

$$\eta = \frac{E_{\text{impact}}}{\sum E_{\text{adhesion}}} \tag{4.4}$$

The impact energy is simply the kinetic energy of the particle assembly (both drug particles and carrier) before collision and is defined as:

$$E_{\text{impact}} = \frac{1}{2}\left(m_c + m_d\right) V_{\text{impact}}^2 \tag{4.5}$$

The work of adhesion forces was calculated for each contact individually, considering the variation of R^* at each contact point, and then these energies were summed up to obtain the total adhesion energy.

The relationship between the dispersion ratio and the energy ratio is plotted in Figure 4.21. The overall trend of this curve shows that, above η around 1×10^4, the dispersion ratio increased sharply with the energy ratio, analogous to the behavior reported by Yang et al. [133] for the collision-induced dispersion ratio of completely spherical carrier particles. In principle, an additional increase in collision velocity results in more detachment of drugs from the carrier particle until the dispersion ratio curve approaches unity for high η values.

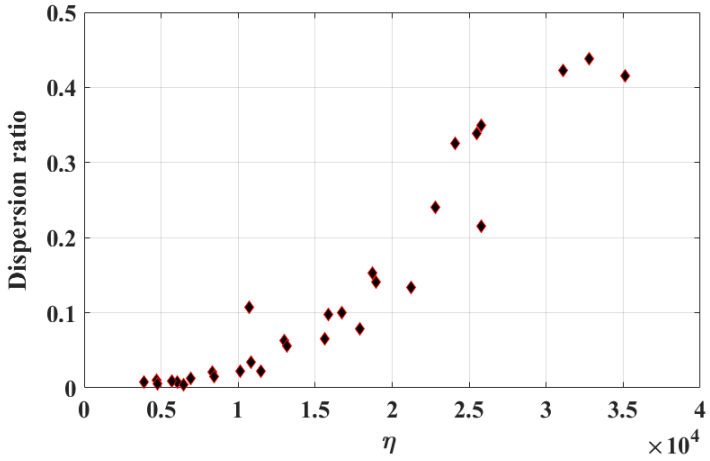

Figure 4.21: The behavior of dispersion ratio versus energy ratio.

4.5.4 Analysis of attached drug particles

The differences in the dispersion ratio of rough carriers were attributed to the net attachment force between drugs and carrier particles, which comprises two factors: (i) the pull-off force that depends on the radius of curvature at contact point, and (ii) the number of established contacts between drug and carrier particles. In order to comprehend the role of these factors in dispersion performance, a 3D spherical histogram was used to represent contact orientation [138]. The cumulative number of drug particles and the total contact force were extracted for this purpose (see Paper IV for more details). Additionally, the number of contact points (or more precisely, the contact area due to the JKR theory) that was established with the carrier was obtained. This information resulted in a histogram that shows the frequency of contact points.

Figure 4.22 illustrates an example of a contact number histogram for a rough carrier particle (Carrier IV). These graphs correspond to the attached drug particles prior to and after collision. It was observed that drug particles were attached to the carrier mostly via one or two contact points. This is natural for a rough carrier surface since it provides greater chances of multiple contact points for the drug particle. After collision, the remaining drug particles were redistributed over the carrier particle and stabilized by falling into surface cavities and forming additional contacts. Two supplementary graphs of contact histogram for a more smooth carrier particle (Carrier II) is provided in Paper IV, Figure 11. Comparison of these two sets of graphs showed that lack of surface asperities on Carrier II (smooth) resulted in the dominance of single contact points between drugs and the carrier surface before collision. However, the tendency of drug particles to establish multiple contacts with carrier was similar for both smooth and rough particles after collision.

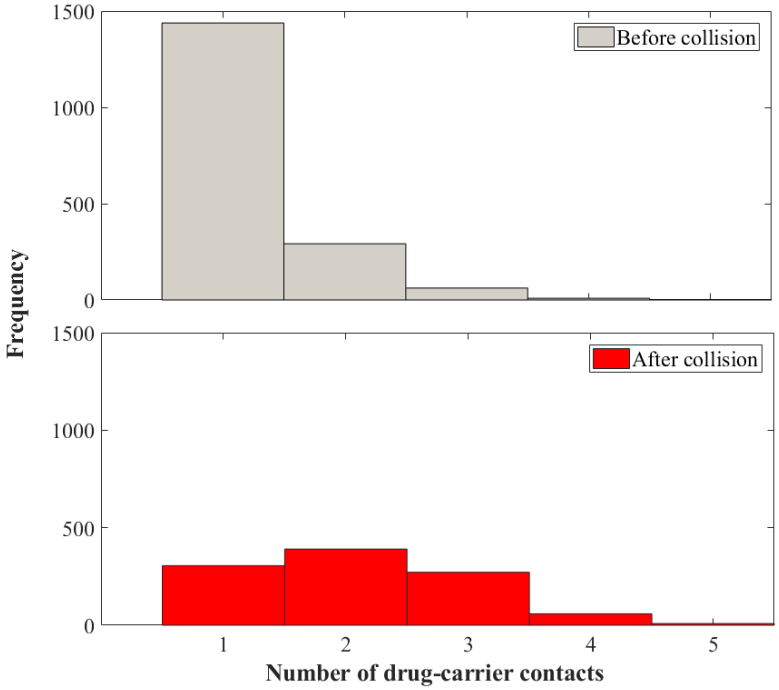

Figure 4.22: An example of contact number histogram between drugs and a rough carrier particle (Carrier IV), prior to and after collision at $V_{impact} = 7\ m/s$.

Another observation concerned the number, location, and adhesion strength of the remaining drug particles after collision. An example of a spherical histogram for the number of attached drugs to a rough carrier particle is illustrated in Figure 4.23. For comparison, a similar set of graphs was reproduced for a relatively smoother carrier particle and is available in Paper IV, Figure 11. Besides the number of drug particles, the magnitude of adhesion forces between drugs and carrier particle was calculated. Their corresponding spherical histogram can be found in Paper IV, Figures 10 and 11.
Analyses of dispersion ratio revealed that the rough carrier particle experienced a higher degree of detachment than the smooth one. The detachment from the rough carrier occurred mostly in the hemisphere facing the wall, and therefore, the spherical histogram shows a strong asymmetrical distribution for the attached drug particles in favor of the opposite hemisphere. However, the detachment from and migration towards the hemisphere adjacent to the wall occurred simultaneously for the smooth carrier. Therefore, the corresponding spherical histogram showed a greater number of attached drug particles in this hemisphere. It was noted that rough carrier particles had a lower adhesion force than the smooth particles. This is because rough carrier particles had more and smaller spherical asperities on the surface, which lowered the magnitude of the adhesion force. Thus, the differences in the adhesion forces and the number of contact points governed a difference in general dispersion performance.

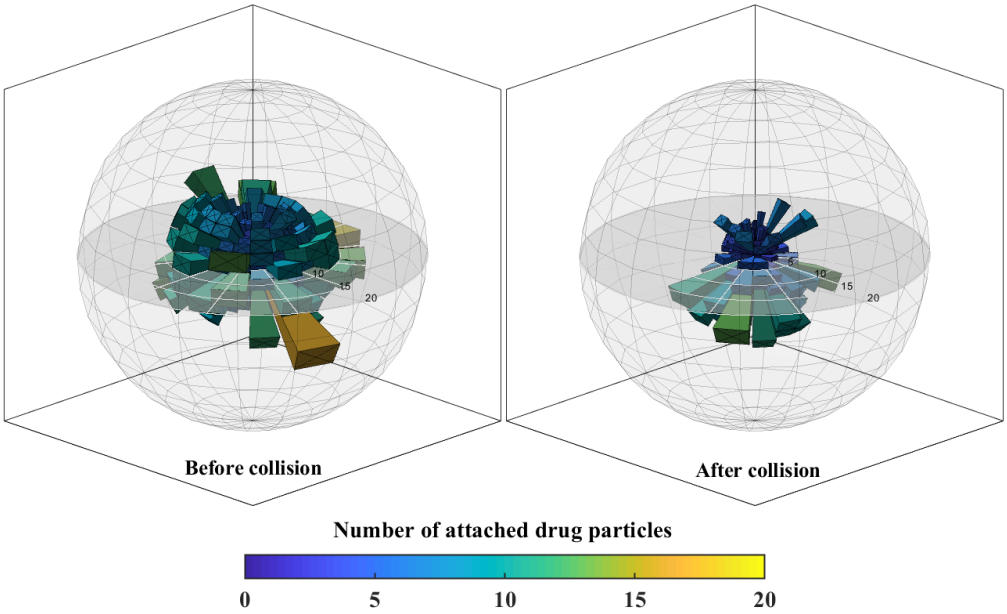

Figure 4.23: Spherical histogram of contact orientation for drug particles attached onto a rough carrier particle (Carrier IV), prior to and after collision at $V_{impact} = 7\ m/s$.

5

Conclusions and outlook

The goal of this research was to devise a general methodology for understanding the complex nature of the adhesive mixing process for inhalation applications and to form a basis for process optimization. The small temporal and spatial scales of the adhesive mixing, on the one hand, and the omnipresent interplay of process variables, on the other hand, required a modeling framework and several quality-assessment tools.
The underlying principle of this framework was to treat the adhesive mixture as a particulate system, the dynamic behavior of which could be modelled by applying Newton's laws of motion to individual particles, i.e. DEM (**Papers I-V**). Several formulation variables were selected in accordance with their significance in the process and within the capacity of the developed model, for parameter studying.

A binary system of adhesive carrier and drug particles was simulated in **Paper I**, and several assessment tools, including a mixing index, were formulated. The simulation captured the essential steps of the adhesive mixing process as described in the literature. One interesting observation was in regards to the compaction of loosely packed drug agglomerates prior to their breakage during shearing.

The binary system was then subjected to parameter studying in **Paper II**. Four regimes in the adhesive mixing process were identified as a function of the two most prominent variables, namely mixing energy and the surface energy of particles. These variables were converted into two dimensionless quantities, the Stokes number (St) and the Λ ratio, and a regime map was created. The former quantity describes the ratio of mixing energy to the energy needed to break the interparticle contacts within drug agglomerates, and the latter one represents the cohesive-adhesive balance. Each regime was characterized by its dominant phenomenon and mixture quality. Three regimes led to undesired mixing behavior:

- In cases with both low St and ratio, carriers were jammed, and random mixing was fairly poor.
- In cases with low St and high ratio, the agglomerates lumped together.
- In cases with high St, the adhesion of drug and carrier broke, carriers remained un-coated, and an abundance of debris was created.

For a given set of particles, it was possible to tune the input energy of the coating devices so that the operation window fell within the desired mixing regime.

As the capabilities of the model expanded, non-spherical particles were incorporated into the simulations of the adhesive mixing process. With this incorporation, focus was shifted to the geometrical attributes of particles, including shape and roughness. A fundamental

step in the adhesive mixing of non-spherical carrier particles was investigated in **Paper III**. The effect of carrier shape factors on the breakage of agglomerates and the pattern of adhesion of drug particles onto a carrier surface were explored. It was found that:

- The smallest scales of particle morphology, i.e. asperities, caused the most significant variation in the extent of the disintegration of agglomerates and, consequently, the number of drugs captured by the carrier.
- The capture ratio was the highest when the collision occurred over smooth and flat zones of the carrier, and it was the lowest when the agglomerate impacted local peaks on the carrier surface.
- The elongation of the carrier was found to largely influence the size of the created fragments after impact. These types of carriers can chop off rather large parts of an agglomerate and create a few, large fragments.

These results reveal a major error when approximating real particles as smooth spheres in fragmentation studies.

The interesting outcomes of the model developed for **Paper III** provided us with the competence to determine the vital role of carrier surface roughness in the dispersion performance of carrier-based DPIs. Therefore, the collision-induced detachment of drug particles from rough carrier particles was studied in **Paper IV**. It was found that dispersion performance (quantified by the number of detached drug particles) is proportional to the root-mean-square of the surface asperity height. The presence of cavities on the surface of rougher particles provides a chance for drugs to establish multiple contact points with the carrier surface.
During collision, the redistribution of drug particles over a carrier surface occurred alongside drug particle detachment. Collision kinetic energy and surface roughness were found to impose a profound effect on these two phenomena. Dispersion behavior versus collision energy is expressed in terms of the dimensionless energy ratio,η, defined as the pre-impact kinetic energy of particles over the work of adhesion required to liberate all fine particles.

An intriguing query in the context of carrier-based DPIs is to mechanistically understand the benefits of ternary formulation over binary ones, as this question has remained open for debate. With the ability of the developed model to create irregular carrier particles with heterogeneous surface activity, the effect of adding fines to adhesive mixing by performing DEM simulations in a simple vibrational mixing cell was addressed in **Paper V**. A log-normal distribution was, therefore, introduced to the surface activity of carriers, and a competing environment for drug and fine particles to occupy more active sites was created. The key findings were:

- The results did not reveal any tendency toward competition, and therefore, the active site theory was contradicted.
- The buffer theory and the agglomeration theory propose the most relevant mechanisms of the available theories on the role of fine excipient particles.
- As the loading ratio of fine particles increases, the drug agglomerate breakage became inefficient, which led to a poor degree of mixing.

We observed that, when large enough, the fine particles prevented the complete breakage of drug agglomerates by sheltering them from carrier collisions. Therefore, the drug

particles that are attached onto a carrier tend to remain in a multilayer rather than a monolayer structure. Even though the collision- or flow-induced dispersion of drug particles was not examined here, it is plausible that such multilayer structures will gain larger momentum and detach easier from the carrier during aerosolization, as proposed in the agglomeration theory. The poor mixing caused by an abundance of fine particles is due to the fact that the inclusion of cohesive fine particles adds up to the tensile strength of the particle assembly and restricts the rotational motion of coarse particles to a great extent.

Finally, we will address some limitations of the present work and provide suggestions for future research.
Despite the vast improvement in understanding and formulation of the contact problem for adhesive particles, the available models have certain shortcomings. A comprehensive contact model for adhesive and rough particles, that may exhibit plastic behavior under compression, is still in demand. The plasticity (i.e. permanent deformation of particles) can be of central importance in modelling the press-on force effect in the formulation process.
The effect of relative humidity and the electric charge build-up, as two general concerns in particle mixing, have not been in the focus of the present research. These two were disregarded since the formulation process for DPIs is normally preformed under controlled conditions, i.e. low relative humidity as the process should resemble dry-coating, and continuous discharge of electrostatic charge. However, even under such conditions, a total absence of these two phenomena is not guaranteed. There are available contact models to incorporate the forces that arise from liquid bridge between contagious particles or the body force in the presence of electric charge into the existing simulation framework.
From the practical implication viewpoint, the dispersion of drug particles during inhalation is the pivotal purpose of the adhesive mixing process. Therefore, it is necessary to develop a full-scale modelling framework wherein the dispersion performance of the adhesive mixture is directly evaluated (i.e. multi-scale modelling for lung dispersion using the CFD-DEM technique).
Last, but certainly not least, the models should be validated with experimental data. An experimental approach helps to identify key variables better and identifies the irrelevant parameters and unrealistic simulation cases to be discarded. However, this is a challenging problem since simulations can only be done on small systems with a limited number of idealized particles, which is difficult to realize in an experimental apparatus.

References

[1] J. Ai, J. F. Chen, J. M. Rotter, and J. Y. Ooi. Assessment of rolling resistance models in discrete element simulations. *Powder Technology*, 206(3):269–282, 2011.

[2] M. Alonso and F. J. Alguacil. Dry mixing and coating of powders. *Revista de Metalurgia*, 35(5):315–328, 1999.

[3] M. Alonso, M. Satoh, and K. Miyanami. Kinetics of fines transfer among carriers in powder coating. *Powder Technology*, 59(3):217–224, 1989.

[4] M Alonso, M Satoh, and K Miyanami. The effect of random positioning on the packing of particles adhering to the surface of a central particle. *Powder Technology*, 62(1):35–40, 1990.

[5] J. E. Andrade, K. W. Lim, C. F. Avila, and I. Vlahinić. Granular element method for computational particle mechanics. *Computer Methods in Applied Mechanics and Engineering*, 241:262–274, 2012.

[6] D. Antypov and J. A. Elliott. On an analytical solution for the damped hertzian spring. *EuroPhysics Letters (EPL)*, 94(5):50004, 2011.

[7] A. K. Ashamawy, B. Sukumaran, and V. Vinh Hoang. Evaluating the influence of particle shape on liquefaction behavior using discrete element method. In *Proceedings of 13th International Offshore and Polar Engineering Conference, ISOPE*, volume 2, pages 542–549.

[8] R. A. Bagnold. Experiments on a gravity-free dispersion of large solid spheres in a newtonian fluid under shear. *Proceedings of the Royal Society of London. Series A. Mathematical and Physical Sciences*, 225(1160):49–63, 1954.

[9] Y. Balagurunathan and E. R. Dougherty. Morphological quantification of surface roughness. *Optical Engineering*, 42(6):1795–1805, 2003.

[10] P. J. Barrett. The shape of rock particles, a critical review. *Sedimentology*, 27(3):291–303, 1980.

[11] P. Begat, D. A. V Morton, J. N. Staniforth, and R. Price. The cohesive-adhesive balances in dry powder inhaler formulations i: direct quantification by atomic force microscopy. *Pharmaceutical Research*, 21(9):1591–1597, 2004.

[12] B. Bhushan. Surface roughness analysis and measurement techniques. In *Modern Tribology Handbook, B*, volume Vol. 1, pages 49–114. CRC press.

[13] H. J. Butt and M. Kappl. *Surface and Interfacial Forces*. John Wiley Sons, Weinheim, Germany, 2009.

[14] A. Castellanos. The relationship between attractive interparticle forces and bulk behaviour in dry and uncharged fine powders. *Advances in Physics*, 54(4):263–376, 2005.

[15] J. Z. Chen, H. Herman, and C. C. Huang. A preliminary model for mechanofusion powder processing. *KONA Powder and Particle Journal*, 15:113–120, 1997.

[16] Y. Chen, M. A. S. Quintanilla, J. Yang, J. M. Valverde, and R. N. Dave. Pull-off force of coated fine powders under small consolidation. *Physical Review E*, 79(4):041305, 2009.

[17] Y. Chen, J. Yang, R. N. Dave, and R. Pfeffer. Fluidization of coated group c powders. *AIChE Journal*, 54(1):104–121, 2008.

[18] A. Chokshi, A. Tielens, and D. Hollenbach. Dust coagulation. *The Astrophysical Journal*, 407:806–819, 1993.

[19] C. J. Coetzee. Review: Calibration of the discrete element method. *Powder Technology*, 310:104–142, 2017.

[20] Y. Cui, S. Schmalfuß, S. Zellnitz, M. Sommerfeld, and N. A. Urbanetz. Towards the optimisation and adaptation of dry powder inhalers. *International Journal of Pharmaceutics*, 470(1-2):120–132, 2014.

[21] Y. Cui and M. Sommerfeld. Forces on micron-sized particles randomly distributed on the surface of larger particles and possibility of detachment. *International Journal of Multiphase Flow*, 72:39–52, 2015.

[22] P. A. Cundall. Formulation of a three-dimensional distinct element model—part i. a scheme to detect and represent contacts in a system composed of many polyhedral blocks. In *International Journal of Rock Mechanics and Mining Sciences Geomechanics Abstracts*, volume 25, pages 107–116. Elsevier.

[23] P. A. Cundall and O. D. L. Strack. A discrete numerical model for granular assemblies. *Geotechnique*, 29(1):47–65, 1979.

[24] A. H. De Boer, H. K. Chan, and R. Price. A critical view on lactose-based drug formulation and device studies for dry powder inhalation: which are relevant and what interactions to expect? *Advanced Drug Delivery Reviews*, 64(3):257–274, 2012.

[25] A. H. De Boer, P. Hagedoorn, M. Hoppentocht, F. Buttini, F. Grasmeijer, and H. W. Frijlink. Dry powder inhalation: past, present and future. *Expert Opinion on Drug Delivery*, 14(4):499–512, 2017.

[26] X. Deng, K. Zheng, and R. N. Dave. Discrete element method based analysis of mixing and collision dynamics in adhesive mixing process. *Chemical Engineering Science*, 190:220–231, 2018.

[27] B. V. Derjaguin. Friction and adhesion. iv. the theory of adhesion of small particles. *Kolloid Zeits*, 69:155–164, 1934.

[28] B. V. Derjaguin, V. M. Muller, and Y. P. Toporov. Effect of contact deformations on the adhesion of particles. *Journal of Colloid and Interface Science*, 53(2):314–326, 1975.

[29] A. Di Renzo and F. P. Di Maio. Comparison of contact-force models for the simulation of collisions in dem-based granular flow codes. *Chemical Engineering Science*, 59(3):525–541, 2004.

[30] B. H. J. Dickhoff, A. H. De Boer, D. Lambregts, and H. W. Frijlink. The effect of carrier surface treatment on drug particle detachment from crystalline carriers in adhesive mixtures for inhalation. *International Journal of Pharmaceutics*, 327(1-2):17–25, 2006.

[31] M. J. Donovan and H. D. C. Smyth. Influence of size and surface roughness of large lactose carrier particles in dry powder inhaler formulations. *International Journal of Pharmaceutics*, 402(1-2):1–9, 2010.

[32] J. Drelich, G. W. Tormoen, and E. R. Beach. Determination of solid surface tension from particle–substrate pull-off forces measured with the atomic force microscope. *Journal of Colloid and Interface Science*, 280(2):484–497, 2004.

[33] P. Du, J. Du, and H. D. C. Smyth. Evaluation of granulated lactose as a carrier for dpi formulations 1: effect of granule size. *AAPS PharmSciTech*, 15(6):1417–1428, 2014.

[34] C. A. Dunber, A. J. Hickey, and P. Holzner. Dispersion and characterization of pharmaceutical dry powder aerosols. *KONA Powder and Particle Journal*, 16:7–45, 1998.

[35] A. Dupré and P. Dupré. *Théorie Mécanique de la Chaleur*. Gauthier-Villars, Paris, 1869.

[36] A. Džiugys and B. Peters. A new approach to detect the contact of two-dimensional elliptical particles. *International Journal for Numerical and Analytical Methods in Geomechanics*, 25(15):1487–1500, 2001.

[37] R. Ehrlich and B. Weinberg. An exact method for characterization of grain shape. *Journal of Sedimentary Research*, 40(1):205–212, 1970.

[38] T. Eidevåg, P. Abrahamsson, M. Eng, and A. Rasmuson. Modeling of dry snow adhesion during normal impact with surfaces. *Powder Technology*, 361:1081–1092, 2020.

[39] M. Ester, H. Kriegel, J. Sander, and X. Xu. A density-based algorithm for discovering clusters in large spatial databases with noise. In *KDD*, volume 96, pages 226–231.

[40] J. K. Eve, N. Patel, S. Y. Luk, S. J. Ebbens, and C. J. Roberts. A study of single drug particle adhesion interactions using atomic force microscopy. *International Journal of Pharmaceutics*, 238(1-2):17–27, 2002.

[41] J. F. Favier, M. H. Abbaspour-Fard, M. Kremmer, and A. O. Raji. Shape representation of axi-symmetrical, non-spherical particles in discrete element simulation using multi-element model particles. *Engineering Computations*, 16(4):467–480, 1999.

[42] J. F. Ferellec and G. R. McDowell. A method to model realistic particle shape and inertia in dem. *Granular Matter*, 12(5):459–467, 2010.

[43] E. Fermi, J. Pasta, S. Ulam, and M. Tsingou. Los alamos report no. Report, 1955.

[44] M. P. Flament, P. Leterme, and A. Gayot. The influence of carrier roughness on adhesion, content uniformity and the in vitro deposition of terbutaline sulphate from dry powder inhalers. *International Journal of Pharmaceutics*, 275(1-2):201–209, 2004.

[45] D. Ganderton. Targeted delivery of inhaled drugs: current challenges and future goals. *Journal of Aerosol Medicine*, 12(s1):S–3–S–8, 1999.

[46] J. Ghaboussi and R. Barbosa. Three-dimensional discrete element method for granular materials. *International Journal for Numerical and Analytical Methods in Geomechanics*, 14(7):451–472, 1990.

[47] M. Ghadiri, R. Moreno-Atanasio, A. Hassanpour, and Antony S. J. *Analysis of Agglomerates Breakage*, volume 12, book section 19, pages 837–872. Springer Science Business Media, 2007.

[48] J. D. Goddard. Continuum modeling of granular media. *Applied Mechanics Reviews*, 66(5):050801, 2014.

[49] D. Golchert, R. Moreno, M. Ghadiri, and J. D. Litster. Effect of granule morphology on breakage behaviour during compression. *Powder Technology*, 143:84–96, 2004.

[50] F. Grasmeijer. *Adhesive mixture inhalation: the cohesion between formulation variables, inhlation variables and dispersion perfromance.* Thesis, 2014.

[51] F. Grasmeijer, H. W. Frijlink, and A. H. De Boer. A proposed definition of the 'activity'of surface sites on lactose carriers for dry powder inhalation. *European Journal of Pharmaceutical Sciences*, 56:102–104, 2014.

[52] F. Grasmeijer, P. Hagedoorn, H. W. Frijlink, and A. H. de Boer. Mixing time effects on the dispersion performance of adhesive mixtures for inhalation. *PloS one*, 8(7), 2013.

[53] J. A. Greenwood and J. B. P. Williamson. Contact of nominally flat surfaces. *Proceedings of the Royal Society of London. Series A. Mathematical and Physical Sciences*, 295(1442):300–319, 1966.

[54] M. Götzinger and W. Peukert. Particle adhesion force distributions on rough surfaces. *Langmuir*, 20(13):5298–5303, 2004.

[55] H. C. Hamaker. The london—van der waals attraction between spherical particles. *Physica*, 4(10):1058–1072, 1937.

[56] J. A. Hersey. Ordered mixing: a new concept in powder mixing practice. *Powder Technology*, 11(1):41–44, 1975.

[57] H. Hertz. Über die berührung fester elastischer körper. *Journal für die Reine und Angewandte Mathematik*, 92:156–171, 1882.

[58] A. J. Hickey and Z. Xu. *Dry Powder Inhalers*, pages 295–322. Springer International Publishing, Switzerland, 2014.

[59] H. Honda, M. Kimura, F. Honda, T. Matsuno, and M. Koishi. Preparation of monolayer particle coated powder by the dry impact blending process utilizing mechanochemical treatment. *Colloids and Surfaces A: Physicochemical and Engineering Aspects*, 82(2):117–128, 1994.

[60] M. Hoppentocht, P. Hagedoorn, H. W. Frijlink, and A. H. De Boer. Technological and practical challenges of dry powder inhalers and formulations. *Advanced Drug Delivery Reviews*, 75:18–31, 2014.

[61] S. S. Hsiau, L. S. Lu, J. C. Chen, and W. L. Yang. Particle mixing in a sheared granular flow. *International Journal of Multiphase Flow*, 31(7):793–808, 2005.

[62] N. Islam, P. J. Stewart, I. Larson, and P. Hartley. Effect of carrier size on the dispersion of salmeterol xinafoate from interactive mixtures. *Journal of Pharmaceutical Sciences*, 93(4):1030–1038, 2004.

[63] J. N. Israelachvili. *Intermolecular and Surface Forces*. Academic Press, third edition, 2011.

[64] S. M. Iveson and J. D. Litster. Growth regime map for liquid-bound granules. *AIChE Journal*, 44(7):1510–1518, 1998.

[65] K. L. Johnson, K. Kendall, and A. D. Roberts. Surface energy and the contact of elastic solids. In *Proceedings of the Royal Society of London A: Mathematical, Physical and Engineering Sciences*, volume 324, pages 301–313. The Royal Society.

[66] M. D. Jones and R. Price. The influence of fine excipient particles on the performance of carrier-based dry powder inhalation formulations. *Pharmaceutical Research*, 23(8):1665–1674, 2006.

[67] M. D. Jones, J. G. F. Santo, B. Yakub, M. Dennison, H. Master, and G. Buckton. The relationship between drug concentration, mixing time, blending order and ternary dry powder inhalation performance. *International Journal of Pharmaceutics*, 391(1-2):137–147, 2010.

[68] W. Kaialy, A. Alhalaweh, S. P. Velaga, and A. Nokhodchi. Effect of carrier particle shape on dry powder inhaler performance. *International Journal of Pharmaceutics*, 421(1):12–23, 2011.

[69] W. Kaialy, G. P. Martin, H. Larhrib, M. D. Ticehurst, E. Kolosionek, and A. Nokhodchi. The influence of physical properties and morphology of crystallised lactose on delivery of salbutamol sulphate from dry powder inhalers. *Colloids and Surfaces B: Biointerfaces*, 89:29–39, 2012.

[70] WH Keesom. Die van der waalsschen kohasionskrafte. *Physikalische Zeit*, 22:129, 1921.

[71] C. Kloss and C. Goniva. Liggghts: a new open source discrete element simulation software. In *Proceedings of The 5th International Conference on Discrete Element Methods, London, UK*, pages 25–26.

[72] S. Krishnan. Volume of a surface triangulation. https://www.mathworks.com/matlabcentral/fileexchange/26982-volume-of-a-surface-triangulation. MATLAB Central File Exchange, Retrieved March 3, 2020.

[73] P. Kulvanich and P. J. Stewart. The effect of blending time on particle adhesion in a model interactive system. *Journal of Pharmacy and Pharmacology*, 39(9):732–733, 1987.

[74] P. M. C. Lacey. Developments in the theory of particle mixing. *Journal of Applied Chemistry*, 4(5):257–268, 1954.

[75] V. N. P. Le, H. Bierend, E. Robins, H. Steckel, and M. P. Flament. Influence of the lactose grade within dry powder formulations of fluticasone propionate and terbutaline sulphate. *International Journal of Pharmaceutics*, 422(1-2):75–82, 2012.

[76] S. Li, J. S. Marshall, G. Liu, and Q. Yao. Adhesive particulate flow: The discrete-element method and its application in energy and environmental engineering. *Progress in Energy and Combustion Science*, 37(6):633–668, 2011.

[77] X. Lin and T.t Ng. Contact detection algorithms for three-dimensional ellipsoids in discrete element modelling. *International Journal for Numerical and Analytical Methods in Geomechanics*, 19(9):653–659, 1995.

[78] E. M. Littringer, A. Mescher, H. Schroettner, L. Achelis, P. Walzel, and N. A. Urbanetz. Spray dried mannitol carrier particles with tailored surface properties–the influence of carrier surface roughness and shape. *European Journal of Pharmaceutics and Biopharmaceutics*, 82(1):194–204, 2012.

[79] M. D. Louey, P. Mulvaney, and P. J. Stewart. Characterisation of adhesional properties of lactose carriers using atomic force microscopy. *Journal of Pharmaceutical and Biomedical Analysis*, 25(3-4):559–567, 2001.

[80] M. D. Louey and P. J. Stewart. Particle interactions involved in aerosol dispersion of ternary interactive mixtures. *Pharmaceutical Research*, 19(10):1524–1531, 2002.

[81] G. Lu, J. R. Third, and C. R. Müller. Critical assessment of two approaches for evaluating contacts between super-quadric shaped particles in dem simulations. *Chemical Engineering Science*, 78:226–235, 2012.

[82] G. Lu, J. R. Third, and C. R. Müller. Discrete element models for non-spherical particle systems: from theoretical developments to applications. *Chemical Engineering Science*, 127:425–465, 2015.

[83] P. Lucas, K. Anderson, and J. N. Staniforth. Protein deposition from dry powder inhalers: fine particle multiplets as performance modifiers. *Pharmaceutical Research*, 15(4):562–569, 1998.

[84] P. Lucas, M. J. Clarke, K. Anderson, M. J. Tobyn, and J. N. Staniforth. The role of fine particle excipients in pharmaceutical dry powder aerosols. In *Respiratory Drug Delivery VI*, volume 243, page 250. Interpharm Press, Inc. Buffalo Grove, IL.

[85] M. Lätzel, S. Luding, and H. J. Herrmann. Macroscopic material properties from quasi-static, microscopic simulations of a two-dimensional shear-cell. *Granular Matter*, 2(3):123–135, 2000.

[86] A Majumdar and B Bhushan. Fractal model of elastic-plastic contact between rough surfaces. *Journal of Tribology*, 113(1):1–11, 1991.

[87] J. S. Marshall. Discrete-element modeling of particulate aerosol flows. *Journal of Computational Physics*, 228(5):1541–1561, 2009.

[88] D. Maugis. Adhesion of spheres: the jkr-dmt transition using a dugdale model. *Journal of Colloid and Interface Science*, 150(1):243–269, 1992.

[89] GF Miller and H Pursey. On the partition of energy between elastic waves in a semi-infinite solid. In *Proceedings of the Royal Society of London A: Mathematical, Physical and Engineering Sciences*, volume 233, pages 55–69. The Royal Society.

[90] R. D. Mindlin. Compliance of elastic bodies in contact. *Journal of Applied Mechanics*, 16:259–268, 1949.

[91] R. D. Mindlin and H. Deresiewicz. Elastic spheres in contact under varying oblique forces. *Trans. ASME, Journal of Applied Mechanics*, 20:327–344, 1953.

[92] G. Mollon and J. Zhao. Fourier–voronoi-based generation of realistic samples for discrete modelling of granular materials. *Granular Matter*, 14(5):621–638, 2012.

[93] G. Mollon and J. Zhao. 3d generation of realistic granular samples based on random fields theory and fourier shape descriptors. *Computer Methods in Applied Mechanics and Engineering*, 279:46–65, 2014.

[94] R. Moreno-Atanasio and M. Ghadiri. Mechanistic analysis and computer simulation of impact breakage of agglomerates: effect of surface energy. *Chemical Engineering Science*, 61(8):2476–2481, 2006.

[95] J. P. Morrissey. *Discrete element modelling of iron ore pellets to include the effects of moisture and fines*. Thesis, 2013.

[96] D. Nguyen, A. Rasmuson, K. Thalberg, and I. Niklasson Björn. Numerical modelling of breakage and adhesion of loose fine-particle agglomerates. *Chemical Engineering Science*, 116:91–98, 2014.

[97] D. Nguyen, A. Rasmuson, K. Thalberg, and I. Niklasson Björn. A breakage and adhesion regime map for the normal impact of loose agglomerates with a spherical target. *AIChE Journal*, 61(12):4059–4068, 2015.

[98] D. Nguyen, A. Rasmuson, K. Thalberg, and I. Niklasson Björn. A study of the redistribution of fines between carriers in adhesive particle mixing using image analysis with coloured tracers. *Powder Technology*, 299:71–76, 2016.

[99] A. W. Nienow, M. F. Edwards, and N. Harnby. *Mixing in the Process Industries*. Butterworth-Heinemann, second edition, 1997.

[100] Z. Ning. *Elasto-plastic impact of fine particles and fragmentation of small agglomerates*. Thesis, 1995.

[101] Z. Ning, R. Boerefijn, M. Ghadiri, and C. Thornton. Distinct element simulation of impact breakage of lactose agglomerates. *Advanced Powder Technology*, 8(1):15–37, 1997.

[102] F. Podczeck. The influence of particle size distribution and surface roughness of carrier particles on the in vitro properties of dry powder inhalations. *Aerosol Science Technology*, 31(4):301–321, 1999.

[103] Y. I. Rabinovich, J. J. Adler, A. Ata, R. K. Singh, and B. M. Moudgil. Adhesion between nanoscale rough surfaces: I. role of asperity geometry. *Journal of Colloid and Interface Science*, 232(1):10–16, 2000.

[104] H. Rumpf. *Particle Technology*, volume 1. London: Chapman Hall, 1990.

[105] I. Saleem, H. Smyth, and M. J. Telko. Prediction of dry powder inhaler formulation performance from surface energetics and blending dynamics. *Drug Development and Industrial Pharmacy*, 34(9):1002–1010, 2008.

[106] P. Selvam and H. D. C. Smyth. Effect of press-on forces on drug adhesion in dry powder inhaler formulations. *Journal of Adhesion Science and Technology*, 25(14):1659–1670, 2011.

[107] S. P. Shah and A. Misra. Liposomal amikacin dry powder inhaler: effect of fines on in vitro performance. *AAPS PharmSciTech*, 5(4):107–113, 2004.

[108] J. Shur, H. Harris, M. D. Jones, J. S. Kaerger, and R. Price. The role of fines in the modification of the fluidization and dispersion mechanism within dry powder inhaler formulations. *Pharmaceutical Research*, 25(7):1631–1640, 2008.

[109] M. Sommerfeld and S. Schmalfuß. Numerical analysis of carrier particle motion in a dry powder inhaler. *Journal of Fluids Engineering*, 138(4):041308, 2016.

[110] M. Sonka, V. Hlavac, and R. Boyle. *Image Processing, Analysis, and Machine Vision*. Cengage Learning, 2014.

[111] D Tabor. Surface forces and surface interactions. *Journal of Colloid and Interface Science*, 58(1):2–13, 1977.

[112] B. M J. Tan, L. W Chan, and P. W. S Heng. Characterizing the surface roughness length scales of lactose carrier particles in dry powder inhalers. *Molecular Pharmaceutics*, 15(4):1635–1642, 2018.

[113] M. J. Telko and A. J. Hickey. Dry powder inhaler formulation. *Respiratory Care*, 50(9):1209–1227, 2005.

[114] K. Thalberg, E. Berg, and M. Fransson. Modeling dispersion of dry powders for inhalation. the concepts of total fines, cohesive energy and interaction parameters. *International Journal of Pharmaceutics*, 427(2):224–233, 2012.

[115] C Thornton. Interparticle sliding in the presence of adhesion. *Journal of Physics D: Applied Physics*, 24(11):1942, 1991.

[116] C. Thornton. *Granular Dynamics, Contact Mechanics and Particle System Simulations*. Particle Technology Series. Springer International Publishing, 2015.

[117] C. Thornton, M. T. Ciomocos, and M. J. Adams. Numerical simulations of agglomerate impact breakage. *Powder Technology*, 105(1):74–82, 1999.

[118] C. Thornton, K. K. Yin, and M. J. Adams. Numerical simulation of the impact fracture and fragmentation of agglomerates. *Journal of Physics D: Applied Physics*, 29(2):424, 1996.

[119] J. M. Ting, M. Khwaja, L. R. Meachum, and J. D. Rowell. An ellipse-based discrete element model for granular materials. *International Journal for Numerical and Analytical Methods in Geomechanics*, 17(9):603–623, 1993.

[120] Z. B. Tong, H. Kamiya, A. B. Yu, H. K. Chan, and R. Y. Yang. Multi-scale modelling of powder dispersion in a carrier-based inhalation system. *Pharmaceutical Research*, 32(6):2086–2096, 2015.

[121] Z. B. Tong, B. Zheng, R. Y. Yang, A. B. Yu, and H. K. Chan. Cfd-dem investigation of the dispersion mechanisms in commercial dry powder inhalers. *Powder Technology*, 240:19–24, 2013.

[122] Z. B. Tong, W. Zhong, A. B. Yu, H. K. Chan, and R. Y. Yang. Cfd–dem investigation of the effect of agglomerate–agglomerate collision on dry powder aerosolisation. *Journal of Aerosol Science*, 92:109–121, 2016.

[123] Y. Tsuji, T. Tanaka, and T. Ishida. Lagrangian numerical simulation of plug flow of cohesionless particles in a horizontal pipe. *Powder Technology*, 71(3):239–250, 1992.

[124] B. van Wachem, K. Thalberg, J. Remmelgas, and I. Niklasson Björn. Simulation of dry powder inhalers: Combining micro-scale, meso-scale and macro-scale modeling. *AIChE Journal*, 63(2):501–516, 2017.

[125] L. Vu-Quoc and X. Zhang. An accurate and efficient tangential force–displacement model for elastic frictional contact in particle-flow simulations. *Mechanics of Materials*, 31(4):235–269, 1999.

[126] O. R. Walton. Application of molecular dynamics to macroscopic particles. *International Journal of Engineering Science*, 22(8-10):1097–1107, 1984.

[127] C. Wellmann, C. Lillie, and P. Wriggers. Comparison of the macroscopic behavior of granular materials modeled by different constitutive equations on the microscale. *Finite Elements in Analysis and Design*, 44(5):259–271, 2008.

[128] J. R. Williams and A. P. Pentland. Superquadrics and modal dynamics for discrete elements in interactive design. *Engineering Computations*, 9(2):115–127, 1992.

[129] K. C. Williams, W. Chen, S. Weeger, and T. J. Donohue. Particle shape characterisation and its application to discrete element modelling. *Particuology*, 12:80–89, 2014.

[130] J. Yang, A. Sliva, A. Banerjee, R. N. Dave, and R. Pfeffer. Dry particle coating for improving the flowability of cohesive powders. *Powder Technology*, 158(1):21–33, 2005.

[131] J. Yang, C. Y. Wu, and M. J. Adams. Dem analysis of particle adhesion during powder mixing for dry powder inhaler formulation development. *Granular Matter*, 15(4):417–426, 2013.

[132] J. Yang, C. Y. Wu, and M. J. Adams. Three-dimensional dem–cfd analysis of air-flow-induced detachment of api particles from carrier particles in dry powder inhalers. *Acta Pharmaceutica Sinica B*, 4(1):52–59, 2014.

[133] J. Yang, C. Y. Wu, and M. J. Adams. Dem analysis of the effect of particle–wall impact on the dispersion performance in carrier-based dry powder inhalers. *International Journal of Pharmaceutics*, 487(1):32–38, 2015.

[134] P. M. Young, A. Sung, D. Traini, P. Kwok, H. Chiou, and H. K. Chan. Influence of humidity on the electrostatic charge and aerosol performance of dry powder inhaler carrier based systems. *Pharmaceutical Research*, 24(5):963–970, 2007.

[135] P. M. Young, O. Wood, J. Y. Ooi, and D. Traini. The influence of drug loading on formulation structure and aerosol performance in carrier based dry powder inhalers. *International Journal of Pharmaceutics*, 416(1):129–135, 2011.

[136] X. M. Zeng, G. P. Martin, S. K. Tee, A. A. Ghoush, and C. Marriott. Effects of particle size and adding sequence of fine lactose on the deposition of salbutamol sulphate from a dry powder formulation. *International Journal of Pharmaceutics*, 182(2):133–144, 1999.

[137] X. M. Zeng, S. K. Tee, G. P. Martin, and C. Marriott. Improving the delivery efficiency of dry powder inhalers (dpis) by adding fine carrier particles to powder formulations. *Thorax*, 51(S3):A74, 1996.

[138] L. Zhang. *The behaviour of granular material in pure shear, direct shear and simple shear*. Thesis, 2003.

[139] Y. C. Zhou, B. D. Wright, R. Y. Yang, B. H. Xu, and A. B. Yu. Rolling friction in the dynamic simulation of sandpile formation. *Physica A: Statistical Mechanics and its Applications*, 269(2):536–553, 1999.

[140] Y. C. Zhou, B. H. Xu, A. B. Yu, and P. Zulli. Numerical investigation of the angle of repose of monosized spheres. *Physical Review E*, 64(2):021301, 2001.

[141] Y. C. Zhou, B. H. Xu, A. B. Yu, and P. Zulli. An experimental and numerical study of the angle of repose of coarse spheres. *Powder Technology*, 125(1):45–54, 2002.